Tracing interaction between hydrocarbon and groundwater systems with isotope signatures preserved in the Anyue gas field, central Sichuan Basin, China

Yan Li [a,c], Shengfei Qin [b], Yunpeng Wang [c,†], Greg Holland [d], Zheng Zhou [a,*]

[a] Lancaster Environment Centre, Lancaster University, LA1 4YQ, UK

[b] Research Institute of Petroleum Exploration & Development (RIPED), PetroChina, Beijing, 100083, China

[c] State Key Laboratory of Organic Geochemistry, Guangzhou Institute of Geochemistry, Chinese Academy of Sciences, 510640, China

[d] Department of Earth and Environmental Sciences, The University of Manchester, M13 9PL, UK

* Corresponding author. Email address: z.zhou4@lancaster.ac.uk (Zheng Zhou)

† Co-corresponding author. Email address: wangyp@gig.ac.cn (Yunpeng Wang)

Abstract

Anyue gas field is a large gas field located in the central Sichuan Basin, China. Although many studies have been carried out previously, the formation mechanism of this field is unclear and currently under debate. To better understand the accumulation history, the role that groundwater plays in transporting hydrocarbons within sedimentary basins and water-gas interactions, stable and noble gas isotopes were measured in thirteen free gas samples from the Anyue gas field. In addition, nine formation water samples and five reservoir bitumen samples were analyzed for stable carbon isotopes. $\delta^{13}C(CH_4)$ values in the gas samples range from -35.0 to -32.6‰, showing evidence of thermogenic origin. $\delta^{13}C$ values among three different types of samples (free gases, water-dissolved gases and reservoir bitumen) show a pattern that cannot be explained by oil cracking followed by free gas accumulation. It suggests the occurrence of gas-groundwater interaction in the Anyue field. Free gas samples can be divided into 2 distinct groups by their geographical locations and stratigraphical source formations. $^{3}He/^{4}He$ ratios (R/R_a) in group 1 and group 2 samples range from 0.0118 to 0.0132 and 0.0115 to 0.0256, respectively, indicating He is mainly derived from the crust. $^{20}Ne/^{22}Ne$ and $^{21}Ne/^{22}Ne$ ratios suggest a mixing between the air and crust sources. $^{40}Ar/^{36}Ar$ ratios ranging from 1658 to 2019 and 2168 to 5973 in group 1 and group 2 samples, respectively, are significantly higher than the air value of 298.6. In comparison, heavier noble gas (Kr and Xe) isotopic compositions are predominantly air-like. The relative enrichment of ^{4}He and $^{21}Ne^*$ in group 1 samples can be possibly explained by preferential release of light noble gases in a low temperature environment. Samples in group 2 show a good fit to the solubility-controlled Rayleigh fractionation model, suggesting the presence of an open system degassing of gases from the groundwater. The excess heavy noble gases in natural gas samples can be attributed to the addition of sedimentary components from the source rocks during geological evolution. ^{4}He groundwater ages considering in-situ production and external flux indicate the addition of

young groundwater into the Anyue gas field. Low gas-groundwater ratios and high $CH_4/^{36}Ar$ ratios suggest that only a small portion of the gases in the current Longwangmiao reservoir of Anyue gas field has been in contact with the relatively young groundwater. Based on the noble gas and stable carbon isotope results in all samples, we propose a two-stage gas and groundwater interaction process during the gas preservation and accumulation history in the Anyue gas field in China.

Keywords: Noble gases; Hydrocarbon gases; Groundwater age; Gas-water ratio; Gas groundwater interaction

1. Introduction

Groundwater plays a critical role in hydrocarbon formation, transportation and preservation through the hydrocarbon systems from source rocks to reservoirs (Kennedy et al., 1985; Ballentine et al., 1991; Pinti and Marty, 1995; Zhou et al., 2005; Barry et al., 2017; Wen et al., 2017; Barry et al., 2018; Byrne et al., 2018a). For example, groundwater can not only bring microbes into previously sterilized subsurface environments to generate biogenic hydrocarbons, but also dissolve the hydrocarbons by processes such as water washing, carrying them into trapping structures (Colwell et al., 1997; Onstott and Tseng, 1997; Walvoord et al., 1999; Zhou et al., 2005; Zhou and Ballentine, 2006; Schlegel et al., 2011). Moreover, the properties of hydrocarbon reservoirs (pore creation and destruction) can be significantly affected by interactions with associated water (Summa, 1995; Williams et al., 1997). However, a good understanding of subsurface fluids dynamics, particularly the relationship between groundwater and hydrocarbon migration and accumulation, remains elusive.

Previous work has shown that conventional geochemical tools, such as biomarkers, stable isotopes (e.g. $\delta^{13}C(CH_4)$) and vitrinite reflectance analysis, can provide important information about characteristics of source rocks, such as kerogen types and thermal maturity, allowing further investigation on burial and thermal histories of sedimentary basins (Dow, 1977; Schoell, 1980; Whiticar et al., 1986; Schoell, 1988; Tilley and Muehlenbachs, 2006; Dai et al., 2014; Li et al., 2015; Barry et al., 2016). For example, by combining existing carbon isotope data with new isotope measurements in tight gas and shale gas samples from different petroleum systems in North America, three different stages of shale gas maturation have been proposed (Tilley and Muehlenbachs, 2013). The reversed trend of carbon isotopic composition ($\delta^{13}C$ (CH_4) > $\delta^{13}C$ (C_2H_6) > $\delta^{13}C$ (C_3H_8)) can not only be explained by mixing between gases from different sources and thermal maturities, but also by Rayleigh fractionation during redox reactions (Burruss and Laughrey, 2010). In addition, molecular indicators, such as benzocarbazoles in hydrocarbon reservoirs, have been used to quantify the secondary oil migration distances (Larter et al., 1996). Furthermore, determination of Pb isotopes in crude oils can also help to better understand oil formation, maturation, migration and oil-rock interaction during transportation and storage (Fetter et al., 2019). However, limited geochemical techniques are available to constrain the possible subsurface mechanisms that affect hydrocarbon migration processes as well as the geological conditions of reservoirs.

Noble gas isotopes have been shown to be effective tracers for subsurface fluid interactions because they are relatively low in abundance and chemically inert (Kennedy et al., 2002; Kipfer et al., 2002; Ozima and Podosek, 2002; Holland and Ballentine, 2006; Byrne et al., 2018b; Cao et al., 2018; Zhang et al., 2019). Noble gases associated with subsurface fluids can be derived from three main terrestrial sources: atmosphere, crust and mantle. Firstly, Air Saturated Water (ASW) is the main reservoir for atmosphere-derived noble gases (e.g. ^{20}Ne, ^{36}Ar, ^{84}Kr and ^{132}Xe). They are introduced into the crustal fluid systems by either being

dissolved in groundwater during recharge or as pore waters during sediment deposition (Torgersen and Kennedy, 1999). Notably, there is no significant radiogenic production for these noble gas isotopes in the subsurface. Secondly, radiogenic noble gases (e.g. ^{4}He, ^{40}Ar, and ^{21}Ne) are generated within the crust, which are associated with the radioactive decay of K, U and Th (Ozima and Podosek, 2002). Thirdly, the partial melting in the mantle related to crustal extension results in the occurrence of mantle-derived noble gases (e.g. ^{3}He) (Battani et al., 2000). Among all three major sources of noble gases, atmosphere-derived and crustal radiogenic noble gases dominate in hydrocarbon systems (Ballentine et al., 1991; Ballentine and Sherwood Lollar, 2002; Kennedy et al., 2002; Barry et al., 2016). These differently sourced noble gases have distinct isotopic compositions and relative abundance patterns, allowing the noble gas contributions from each source to be resolved.

Hydrocarbon systems can be categorized into conventional hydrocarbon systems and unconventional hydrocarbon systems. Compared to conventional natural gas reservoirs (e.g. sandstone or carbonate), unconventional natural gas systems (e.g. shale gas) are generated in situ with little secondary migration taking place, suggesting noble gas signatures are expected to be less affected by basin scale fluid flow regimes (Wen, 2017). Byrne et al. (2018b) has documented ^{4}He concentrations measured in several natural gas fields (both conventional and unconventional systems), suggesting conventional systems have relatively higher ^{4}He concentrations compared to unconventional systems, although there is an overlap between these two groups. High ^{4}He concentrations in conventional gas systems can be accounted for by the addition of radiogenic noble gases from large-scale aquifer systems during the secondary migration (Ballentine et al., 1991; Ballentine et al., 1996). Since noble gases are more soluble in oil and gas than in water (Crovetto et al., 1982), noble gases dissolved in water can preferentially partition into the oil and gas phase during fluid interaction, resulting in strong depletion of noble gases in the groundwater that has interacted with a natural gas or oil phase.

For example, the partitioning of ^{20}Ne and ^{36}Ar between groundwater and oil phase has been used to estimate the volume of oil that interacted with groundwater (Ballentine et al., 1996). Noble gas elemental abundances can be significantly modified by physical processes, such as mixing and diffusion, and partitioning between different fluids and phases, e.g. groundwater, oil, gas and igneous melt, which can then be used to identify the mechanisms that control the transport and emplacement of fluids from these sources into the accumulating reservoirs (Kennedy et al., 1985; Ballentine et al., 1991; Lollar et al., 1994; Zhou et al., 2005; Zhou et al., 2012). Therefore, investigation into generation, migration, and mixing in the hydrocarbon reservoirs can not only provide useful strategies for the exploration and production of petroleum sources, but also raise public awareness of associated environmental issues, such as water contamination (Darrah et al., 2014).

Sichuan Basin is one of the most important on-shore gas producing areas with several different sets of hydrocarbon reservoirs in China. More than 20 commercial oil and gas fields have been discovered in the Sichuan Basin over 60 years, with an estimated annual gas production of 10 billion m^3 (Wei et al., 2008). Geological studies regarding hydrocarbon systems such as source rocks, reservoirs and tectonic activities in the Sichuan Basin have been well documented in many studies (Wei et al., 2008; Dai et al., 2012; Wang et al., 2013; Dai et al., 2014). However, the role of groundwater in gas generation, migration and accumulation processes remains unclear. In this study, both stable carbon and noble gas isotopic data in natural gas samples from the Anyue gas field in the central Sichuan Basin, China are presented. The aims of this study are to 1) identify and quantify the involvement of atmosphere-, crustal-, and mantle-derived noble gases associated with hydrocarbon generation, migration and accumulation processes; 2) characterize the physical processes responsible for noble gas emplacement into hydrocarbon systems during geological timescales, thereby better understand the role of groundwater in the transfer of hydrocarbons within sedimentary basins;

and 3) provide new insights into the evolution of petroleum systems, such as natural gas genesis and transportation, subsurface fluid provenance and fluid flow, which can greatly benefit both academic research and industry in future petroleum investigation and exploration.

2. Geological setting and sample locations

2.1. Geological background of Sichuan Basin

The Sichuan Basin, with an area of 190,000 km^2, is a large and ancient hydrocarbon-bearing superimposed basin located in the western region of the Yangtze craton in China. The basin is a late Triassic foreland basin overlying Sinian-Middle Triassic (Z1-T2) passive continental margin (Li et al., 2013; Liang et al., 2014; Li et al., 2015). It is surrounded by the Micang and Daba mountains in the north, the Daliang mountains in the south, the Longmen and Qionglai mountains in the west and Qiyao mountains in the east (Zhai, 1989; Zou, 2013; Dai et al., 2014) (Fig. 1). Tectonically, the Sichuan Basin can be divided into East, South (including South and Southwest), West and Central Sichuan gas-oil accumulation zones, separated by the Longquanshan fault in the west and the Huayingshan fault in the east (Ma et al., 2008; Wang et al., 2013; Ni et al., 2014).

The sediments in the basin have experienced five main orogenies: the Caledonian, Hercynian, Indosinian, Yanshanian and Himalayan orogenies (Li et al., 2005). The basement rock of the Sichuan Basin was formed around 800 Ma ago. During early Caledonian movement, a thick succession of marine carbonates was deposited overlying the basement (Yang et al., 2018) and Sinian and Cambrian source rock generated oil for the first time. The Leshan-Longnvsi paleohigh was formed in the middle of the basin at the end of the Silurian (Zhai, 1989). Due to uplifting of the whole basin in the late Caledonian and early-middle Hercynian orogenies, the Silurian, Devonian and Carboniferous strata were absent and the early paleo-oil

174 pools in the paleohigh were eroded (Fig. 2). In the late Hercynian and Indosinian movement,
175 the Sinian and Lower Cambrian source rocks in the axial part of the palaeohigh entered peak
176 oil generation stage for the second time, therefore paleo-oil pools formed again. Marine
177 transgression occurred during the late Permian – early Triassic period which had led to the
178 deposition of 300 – 500 m of platform carbonates. They formed several important source rocks
179 in the basin, such as the Upper Permian Longtan formation (P_2l) and the Changxing formation
180 (P_2c) (Hao et al., 2008; Zhu et al., 2011; Jin et al., 2014). In Early-Middle Jurassic, large
181 amounts of condensate oil and wet gas were produced. Then, the Sichuan Basin entered into
182 oil-cracking dry gas stage during the late Yanshanian movement, and the paleo-gas pools
183 gradually formed. The Himalayan orogeny caused the uplifting in the Sichuan Basin, resulting
184 in the end of hydrocarbon generation (Yuan et al., 2012; Xu et al., 2014; Yang et al., 2016).
185 The Leshan-Longnvsi paleouplift was shifted to the current location of the Weiyuan gas field
186 as a new structural high after uplifting by about 4000 m. The eastern part of the paleo-uplift
187 was much less deformed, for example, Gaoshiti and Moxi structures were relatively stable with
188 uplifting an amplitude of about 2500 m (Qin et al., 2018).

189

190 **2.2. Study area**

191 Anyue gas field is located in the eastern part of the axial region of Leshan-Longnvsi
192 paleohigh in central Sichuan Basin (Wei et al., 2014). The strata in the Anyue gas field from
193 top to bottom are Jurassic, Triassic, Permian, Ordovician, Cambrian and Sinian. Several
194 primary gas reservoirs in the Anyue gas field are distributed in the Sinian Dengying formation,
195 Lower Cambrian Longwangmiao formation, Lower Triassic Jialingjiang formation, Middle
196 Triassic Leikoupo formation and Upper Triassic Xujiahe formation (Tang et al., 2008; Ding et
197 al., 2018; Qin et al., 2018; Zhao et al., 2018).

198 The Middle Triassic Leikoupo formation conformably overlies the Lower Triassic
199 Jialingjiang formation and unconformably underlies the Upper Triassic Xujiahe formation
200 (Ding et al., 2018; Jiang et al., 2018). The Leikoupo formation is composed of multiple cyclic
201 carbonates and evaporites. Based on lithology, sedimentary cycle and reservoir development,
202 Leikoupo formation can be divided into four members from bottom to top (Lei-1 (T_2l_1), Lei-2
203 (T_2l_2), Lei-3 (T_2l_3) and Lei-4 (T_2l_4)). Lei-1 (T_2l_1) mainly consists of gypsum with limestone
204 and dolomite; Lei-2 (T_2l_2) contains limestone and gypsum; Lei-3 (T_2l_3) is characterized by
205 limestone, argillaceous limestone and dolomitic limestone in the lower part, dolomitic gypsum
206 or gypsum in the middle part, and limestone and dolomitic limestone in the upper part and Lei-
207 4 (T_2l_4) is composed of dolomite, gypsum dolomite and gypsum in the lower part, gypsum
208 dolomite in the middle part, and algae dolomite, micrite dolomite and grain dolomite in the
209 upper part (Zhu et al., 2011; Ding et al., 2018; Jiang et al., 2018; Tian et al., 2019). Gases in
210 the Middle Triassic in the study area are thought to have an Upper Permian Longtan coal source
211 with R_o value of 1.0 – 2.2% (Huang et al., 1997; Cai et al., 2003).
212 The Lower Triassic Jialingjiang formation is characterized by a mixing of carbonates,
213 siliciclastics, and evaporites, which includes 5 different members from bottom to top (Jia 1(T_1j_1)
214 to Jia 5 (T_1j_5)) (Tang et al., 2008; Tan et al., 2011; Zhao et al., 2018). During the Early Triassic
215 Jialingjiang time interval, the Moxi area was located in the central part of the Upper Yangtze
216 Craton marine basin (Wang, 1985; Tan et al., 2011). A general marine transgression occurred
217 during the earliest T_1j_1 time interval, resulting in the predominant deposition of marine
218 carbonates. Due to a general marine regression and frequent sea level fluctuations, T_1j_2 is
219 characterized by marine carbonates and evaporites, with some terrestrial clastic rocks (Tan et
220 al., 2011). T_1j_3 is dominated by limestone while T_1j_4 and T_1j_5 members are composed of
221 anhydrite, dolostone, limestone, and salt (Tang et al., 2008; Zhao et al., 2018). Gases in the

Lower Triassic were produced by Triassic carbonate source rocks. The maturity of Triassic carbonate source in Sichuan basin is around 1.2 – 2.0% R_o (Dai et al., 1997; Cai et al., 2003).

The lower Cambrian Longwangmiao formation of the Anyue gas field was discovered in central Gaoshiti-Moxi paleo-uplift in 2013, with proven gas reserves of 4403×10^8 m^3 (Zhou et al., 2015). The Longwangmiao formation is dominated by crystalline dolomite, grain dolomite, forming a regional high quality dolomite reservoir (Chen et al., 2017). The Longwangmiao formation gas reservoir has a high temperature of up to 150 °C and ultrahigh pressure with a pressure coefficient of 1.5 – 1.7 (Qin et al., 2018). The predominant source rocks in this field are black mudstone and shale of Lower Cambrian Qiongzhusi formation (kerogen type I), with an average TOC value of 1.95% (Wei et al., 2015; Qin et al., 2018). They remain at high over-mature stage with R_o values up to 2.86% (Yuan et al., 2012). Middle Cambrian Gaotai formation is mainly composed of siltstone. Gypseous dolomite and mudstone served as the direct caprocks in the Longwangmiao formation of the Anyue gas field (Qin et al., 2018).

3. Sample collection and analytical techniques

Three types of samples (thirteen free gas samples, nine formation water samples, five reservoir bitumen samples) from the Anyue gas field (Fig. 1) were collected for this study. Based on geographical locations and stratigraphical source formations, we divided sample wells into two groups. Gas samples (Mo 144 and Mo 004-H9) in group 1 were collected from the first member of the Middle Triassic Leikoupo formation of Anyue gas field while gas samples (Mo 005-H9 and Mo 005-H10) in group 1 were collected from the second member of the Lower Triassic Jialingjiang formation of Anyue gas field. Nine free gas samples (Moxi 13, Moxi 9, Moxi 12, Gaoshi 2, Moxi 204, Moxi 11, Moxi 8, Moxi 008-H1 and Moxi 008-7-H1) in group 2 were collected from the Lower Cambrian Longwangmiao formation of Anyue gas

247 field. Nine formation water samples and five bitumen samples (Moxi 13, Moxi 12, Gaoshi 2,
248 Moxi 204 and Moxi 8) were taken from the Longwangmiao formation of Anyue gas field (Fig.
249 1).

250

251 **3.1. Analysis of natural gas composition and stable carbon isotopic composition**

252 The samples of natural gas and formation water in group 2 were taken from the
253 development wells in the Gaoshiti and Moxi structures. To avoid unexpected interferences on
254 the analysis, we selected development wells with high water productions that were in regular
255 operation for an extended period of time without any recent injections. Thirteen free gas
256 samples for gas composition and stable isotope analyses were collected at the well heads using
257 stainless steel cylinders with two high-pressure valves at both ends. During sampling, the gauge
258 at each wellhead was removed and the steel cylinder was connected to the producing pipeline.
259 Natural gas was flushed through the steel cylinder for five minutes prior to sampling in order
260 to remove contamination. Then the valves at the far end of the sample cylinder were closed
261 first, followed by the closure of the valves at the near end of the steel cylinder. As a result,
262 sample cylinders were filled with wellhead natural gas up to the wellhead pressure (70 bar).
263 The formation water samples from gas fields were taken by using 500 ml glass bottles at gas-
264 water separators of the well sites. After sampling, each bottle was sealed with a rubber plug to
265 ensure that the organic components of formation water would not leak during transportation
266 (Qin et al., 2018). Five reservoir bitumen samples were taken from the drilling cores of
267 Gaoshiti-Moxi structures.

268 Gas composition and carbon isotope analyses were carried out at the Key Laboratory
269 of the Research Institute of Petroleum Exploration and Development of PetroChina as
270 described in Qin et al. (2018).

3.2. Noble gas sample collection and analyses

Samples for noble gas analyses were taken at well heads using 10 mm diameter internally polished refrigeration grade copper tubes sealed with stainless steel pinch-off clamps on both ends. In order to minimize the air contamination during the sampling procedure, well gases were allowed to flush through copper tubes for 10 minutes prior to sampling (Zhou et al., 2005; Wen et al., 2017; Byrne et al., 2018a).

Noble gas abundances and isotopic ratios were determined using an Isotopx NGX noble gas mass spectrometer at the subsurface fluid isotope geochemistry laboratory at Lancaster University (Fig. 3). In the laboratory, the sample copper tubes are mounted on an all-metal ultra high vacuum (UHV) system designed specifically for the extraction, purification and separation of noble gases. First, a mixed gas sample was transferred into a calibrated volume of 69.4 cm^3 (M7-M8-M9 section) containing a Baratron monometer at lab temperature. After expansion and dilution, approximately 0.5 cc STP sample gases were isolated and introduced to a pre-heated Ti-sponge furnace at 800 °C for 20 minutes. Then, the furnace was removed, and the Ti-sponge was left to cool down to room temperature for another 20 minutes. An external water bath can be used to help cool down the Ti-sponge when needed. After cooling, the sample was subsequently expanded into the prepline fitted with two GP-50 Ti-Zr alloy gas getters at different temperatures for 15 minutes. One getter close to A2 was held at 350 °C while the other one close to A7 remained at room temperature. Finally, by using a combination of a titanium sponge and two getters, the majority of reactive gases (hydrocarbons, H_2S, CO_2, CO, etc.) in the sample can be broken down and removed from the system with no effect on noble gases.

After the removal of reactive gases, the mixture of "pure" noble gases (He, Ne, Ar, Kr and Xe) needed to be separated into single noble gas species before measurement, which was done by using cryogenic traps. First, heavy noble gases (Ar, Kr and Xe) were trapped onto an

activated charcoal cold finger immersed into an external liquid nitrogen bath for 15 minutes. The remaining gases (He and Ne) were absorbed onto a cryogenic cold trap which was pre-cooled at 10 K for 15 minutes. The releasing temperatures for He and Ne on the cryotrap are 50 K and 95 K, respectively. Once the Ne isotope measurement was finished and the line was pumped, the charcoal trap was warmed to 210 K for 15 minutes. The previously 'trapped' Ar and Kr were subsequently released and expanded into the line. After several expansion and dilution cycles, a small aliquot of Ar and Kr was isolated and simultaneously inlet into the mass spectrometer for abundance and isotopic analyses. Finally, Xe was released by heating the charcoal at 450 K for 10 minutes prior to Xe isotope determination (Li, 2019).

The ^{4}He, ^{20}Ne and ^{40}Ar isotopes were measured using a Faraday detector while the remaining isotopes were counted on an electron multiplier. A known amount of air standard and a procedural blank were conducted following the same procedure of the sample measurement prior to each sample run. The noble gas elemental abundances for each sample were calculated by normalizing to those of air standards after blank correction. The procedural blanks of major isotopes (^{4}He, ^{20}Ne, ^{40}Ar, ^{84}Kr and ^{132}Xe) account for 0.10, 0.11, 1.59, 2.51 and 1.62% of air standard signals, respectively. Due to the low abundance of He in the atmosphere, the air standard for noble gas measurements at Lancaster University was taken from a gas cylinder filled with a mixture of He spike and Air. The He spike is HESJ-standard with the estimated air normalizing $^{3}He/^{4}He$ ratio of 20.63 ± 0.10 (Matsuda et al., 2002). During Ne abundance and isotope analysis, appropriate mass peaks were monitored to correct for interferences caused by doubly charged ions of $^{40}Ar^{++}$ and $^{44}CO_2^{++}$ on ^{20}Ne and ^{22}Ne, respectively. ^{4}He, ^{20}Ne, ^{36}Ar, ^{84}Kr, and ^{132}Xe abundances had typical uncertainties of 1.6, 1.7, 1.7, 3.6 and 2.5%, respectively. All uncertainties are at ±1σ level of confidence. Errors include statistical analytical error, blank error, air standard reproducibility, the expansion volume uncertainty and mass spectrometer sensitivity stability.

4. Results

All gas samples collected from the Anyue gas field were analyzed for their noble gas abundance and isotopic composition, as well as their major gas composition and stable carbon isotopes. In addition, nine formation water samples and five reservoir bitumen samples from the Longwangmiao formation of the Anyue gas field were also analyzed for stable carbon isotopic composition.

4.1. Major gas species and stable carbon isotopes

CH_4 is the predominant gas in gas samples from the Anyue gas field, with the abundances varying from 98.81 to 99.24% and 98.73 to 99.87% in group 1 and 2 samples, respectively. The remaining gases observed in group 1 samples are C_2H_6 (0.16 – 0.21%), O_2 (0.10 – 0.18%) and N_2 (0.44 – 0.81%). Gas samples in group 2 contain C_2H_6 (0.04 – 0.14%), CO_2 (0.05 – 0.38%) and N_2 (0.33 – 0.95%) (Table 1). The dryness coefficient (C_1/C_1-C_5) represents the percentage of methane relative to the sum of all hydrocarbons measured in samples, which is widely used to identify the origin of natural gases. Generally, the dryness coefficient of pyrolysis-originated gas would increase as thermal evolution proceeds. The dryness coefficient in Anyue gas field is up to 0.9996, indicating that this study area has experienced a high-over high maturity stage. This is in good agreement with the thermal history shown in Fig. 2.

Gas samples in group 1 have $\delta^{13}C(CH_4)$ and $\delta^{13}C(C_2H_6)$ values ranging from -35.0 to -34.6‰, and -34.6 to -32.1‰, respectively. $\delta^{13}C(CH_4)$ and $\delta^{13}C(C_2H_6)$ values in group 2 samples range from -34.2 to -32.6‰ and -32.5 to -30.5‰, respectively. According to the major gas composition and carbon isotope data described above, the natural gas in the Anyue gas field is most likely thermogenic in origin, which is consistent with previous studies (Dai et al., 2012; Chen et al., 2017; Qin et al., 2018).

Fig. 4 shows a comparison of $\delta^{13}C$ values among three different types of samples (free gases, water-dissolved gases and bitumen) in group 2 samples from the Anyue gas field. $\delta^{13}C(CH_4)$ in the free gas samples, formation water samples and reservoir bitumen samples range from -34.2 to -32.6‰, -31.4 to -24.4‰ and -35.7 to -34.7‰, respectively. Water-dissolved gas samples taken from formation water have much less negative $\delta^{13}C(CH_4)$ values than free gas samples, while the carbon isotope $\delta^{13}C(CH_4)$ in reservoir bitumen is much more negative than those of free CH_4 in the gas reservoirs.

Natural gas in the Longwangmiao reservoir of the Anyue gas field is generally considered to be the products of secondary oil cracking while solid bitumen is generated from high-molecular substances with an aromatic nucleus due to the condensation polymerization (Qin et al., 2018). During the formation of bitumen and alkane gas, carbon isotopes undergo fractional distillation, which leads to their carbon isotopic ratios following the order of $\delta^{13}C_{bitumen} > \delta^{13}C_{crude\ oil} > \delta^{13}C_{alkane\ gas}$ (Dai et al., 1992).

The measured $\delta^{13}C$ values in free gas samples and reservoir bitumen samples are isotopically reversed compared to the expected direction. Dissolution into water followed by exsolution back into gas phase could fractionate $\delta^{13}C$ to a higher value as demonstrated in the water-dissolved gas samples in this study (Fig. 4). The $\delta^{13}C$ pattern in the free gas and bitumen samples could possibly be explained by gases previously dissolved in the formation water and exsolved from the groundwater system during geological timescale and migrated into gas reservoirs in the form of free gas, resulting in the relative enrichment of $\delta^{13}C(CH_4)$ in free gas samples with respect to that of bitumen (Leonte et al., 2018). Therefore, $\delta^{13}C(CH_4)$ results in these three types of samples show evidence that a water gas interaction possibly occurred in the Anyue gas field. This interaction is further discussed with noble gas data in Section 5.7.

370 **4.2. Noble gases**

371 Noble gas abundances and isotopic compositions in free gas samples are summarized
372 in Tables 2 and 3.

373 **4.2.1. Helium**

374 ^{4}He concentrations in group 1 and group 2 samples vary from 9.01×10^{-5} to 1.59×10^{-4}
375 and 9.67×10^{-5} to 1.42×10^{-4} cm^3STP/cm^3, respectively (Table 2). Measured $^{3}He/^{4}He$ ratios R,
376 are normalised to the atmospheric $^{3}He/^{4}He$ ratio R_a of 1.384×10^{-6} (Ozima and Podosek, 2002).
377 The $^{3}He/^{4}He$ ratio in the crust is 0.02 R_a and 6 – 8 R_a in the upper mantle depending on the
378 location in the mantle (Ozima and Podosek, 2002). R/R_a values measured in samples from
379 group 1 and group 2 samples range from 0.0118 to 0.0132 and 0.0115 to 0.0256, respectively
380 (Table 3), suggesting a strong crustal signature (Ballentine and Burnard, 2002; Ozima and
381 Podosek, 2002). $^{4}He/^{20}Ne$ ratios in samples (up to 16000) are much higher than the atmospheric
382 value of $^{4}He/^{20}Ne = 0.288$, indicating that the atmospheric He contributions are negligible (Fig.
383 5). Assuming $R/R_a = 8.0$ and 0.02 are endmembers for mantle and crustal-radiogenic sources,
384 respectively (Ballentine and Burnard, 2002; Dunai and Porcelli, 2002), then ^{4}He in all the
385 samples are almost entirely crustal derived (> 99%). The crust derived He in samples indicates
386 tectonically stable conditions during the formation of the Sichuan Basin, which prevented
387 significant volatile contributions from the mantle (Ni et al., 2014; Wei et al., 2014).

388 **4.2.2. Neon**

389 Gas samples in group 1 and group 2 have ^{20}Ne concentrations ranging from 9.52×10^{-10}
390 to 2.11×10^{-9} and 7.01×10^{-10} to 2.25×10^{-9} cm^3STP/cm^3, respectively (Table 2). ^{20}Ne is
391 predominantly derived from groundwater previously equilibrated with atmosphere or trapped
392 pore waters, then incorporated into the subsurface fluid systems via phase interaction. In group
393 1 samples, $^{20}Ne/^{22}Ne$ and $^{21}Ne/^{22}Ne$ ratios change from 9.46 to 10.14 and 0.0507 to 0.0580,

394 respectively. $^{20}Ne/^{22}Ne$ and $^{21}Ne/^{22}Ne$ values in group 2 samples from the Anyue gas fields
395 vary from 8.96 to 9.87 and 0.0442 to 0.0799, respectively (Table 3, Fig. 6).

396 Neon isotope compositions suggest that a two-component mixing process between the
397 air and crust endmembers has occurred in the gas reservoirs. There is also minor addition from
398 mantle components in the samples or potentially a diffusive fractionation process affecting Ne
399 isotopes (Zhou et al., 2005; Zhou et al., 2012; Byrne et al., 2018b; Warr et al., 2018). By taking
400 air, mantle and crustal Ne component endmembers as $^{20}Ne/^{22}Ne_{air} = 9.80$, $^{21}Ne/^{22}Ne_{air} = 0.029$,
401 $^{20}Ne/^{22}Ne_{mntl} = 12.5$, $^{21}Ne/^{22}Ne_{mntl} = 0.06$, $^{20}Ne/^{22}Ne_{crust} = 0.30$ and $^{21}Ne/^{22}Ne_{crust} = 0.52$
402 (Ballentine and Burnard, 2002), it is possible to resolve the contribution of atmospheric, mantle
403 and crustal Ne components. Resolved excess $^{21}Ne^*(^{21}Ne_{rad} + ^{21}Ne_{mntl})$ range from 3.25×10^{-12}
404 to 5.27×10^{-12} cm^3STP/cm^3, which accounts for 46.6% to 65.8% of ^{21}Ne concentrations in
405 group 1 samples. Gas samples in group 2 have $^{21}Ne^*$ varying from 3.27×10^{-12} to 5.67×10^{-12}
406 cm^3STP/cm^3, representing 40.7% to 74.3% of the total ^{21}Ne concentrations.

407 **4.2.3. Argon**

408 Groundwater-derived ^{36}Ar concentrations in two sample groups change from 5.31×10^{-9}
409 to 1.11×10^{-8} cm^3STP/cm^3 and 4.52×10^{-9} to 8.95×10^{-9} cm^3STP/cm^3, respectively. Samples
410 in group 1 and group 2 have $^{40}Ar/^{36}Ar$ ratios varying from 1658 to 2109 and 2168 to 5973,
411 respectively (Table 3, Fig. 7), showing significant deviation from the atmospheric $^{40}Ar/^{36}Ar$
412 value of 298.6 (Lee et al., 2006). Resolved non-atmosphere derived excess ^{40}Ar ($^{40}Ar^*$) can be
413 calculated as below following Ballentine and Burnard (2002) :

$$^{40}Ar^* = {}^{40}Ar_{meas} \times \left[1 - \left(^{40}Ar/^{36}Ar\right)_{air} / \left(^{40}Ar/^{36}Ar\right)_{meas}\right] \quad (1)$$

414 where $(^{40}Ar/^{36}Ar)_{air} = 298.6$ (Lee et al., 2006).

Resolved non-atmosphere derived excess ^{40}Ar(^{40}Ar*) contributes from 82.2 to 86% of the measured ^{40}Ar concentrations in group 1 samples, having ^{40}Ar* concentrations ranging from 9.63×10^{-6} to 1.51×10^{-5} cm^3STP/cm^3. Samples in group 2 have ^{40}Ar* concentrations varying between 1.52×10^{-6} and 2.57×10^{-5} cm^3STP/cm^3, which accounts for up to 95.1% of measured ^{40}Ar concentrations.

4.2.4. Krypton and Xenon

^{84}Kr concentrations in group 1 and group 2 samples from the Anyue field vary from 4.11×10^{-10} to 6.96×10^{-10} and 4.36×10^{-10} to 6.42×10^{-10} cm^3STP/cm^3, respectively (Table 2). Taking an atmospheric $^{86}Kr/^{84}Kr$ ratio of 0.302, measured $^{86}Kr/^{84}Kr$ ratios in all samples are predominantly air-like with an average value of 0.317 (Table 3).

^{132}Xe concentrations change from 4.17×10^{-11} to 6.21×10^{-11} cm^3STP/cm^3 in group 1 samples and 3.53×10^{-11} to 7.28×10^{-11} cm^3STP/cm^3 in group 2 samples (Table 2). Similar to Kr, $^{136}Xe/^{132}Xe$ ratios in samples are indistinguishable from the air value of $^{136}Xe/^{132}Xe$ = 0.3293, varying from 0.3213 to 0.3349 and 0.3218 to 0.3399 in group 1 and group 2 samples, respectively (Table 3).

4.3. Groundwater-derived noble gas components

^{20}Ne, ^{36}Ar, ^{84}Kr and ^{132}Xe are predominantly derived from the atmosphere dissolved in groundwater at recharge (Ballentine et al., 2002). By resolving Ne isotopes from different components, groundwater-derived ^{20}Ne($^{20}Ne^{\dagger}$) represents 66.1 to 96.6% and 64.5 to 98.6% of the total ^{20}Ne concentration for group 1 and group 2 samples, respectively. Calculation shows that only ~ 4.5% of non-atmosphere ^{36}Ar can be resolved in samples from the Anyue natural gas field, hence we made a simplified assumption that ^{36}Ar is entirely groundwater-derived. In addition, ^{84}Kr and ^{132}Xe are assumed to be entirely derived from groundwater as well.

Groundwater-derived noble gas concentrations in this study are assumed to be originated from ASW at 10 °C at an altitude of 400 m, i.e., the mean annual air temperature and average altitude in the central Sichuan Basin, respectively. In addition, a 15 % Ne excess air component is also taken into account for calculation (Stute et al., 1992; Stute et al., 1995; Kipfer et al., 2002). Samples in group 1 exhibit $^{20}Ne^{\dagger}/^{36}Ar$ ratios ranging between 0.122 and 0.184 while group 2 samples have $^{20}Ne^{\dagger}/^{36}Ar$ ratios ranging from 0.092 to 0.228 (Table 3, Fig. 8). The relatively lower $^{20}Ne^{\dagger}/^{36}Ar$ ratios compared to the ASW $^{20}Ne/^{36}Ar$ ratio = 0.156 in our study area may suggest the occurrence of phase interactions among different fluid systems in the crust. Measured $^{84}Kr/^{36}Ar$ ratios and $^{132}Xe/^{36}Ar$ ratios in group 1 samples vary from 0.055 to 0.077, and 0.0055 to 0.0079, respectively. Group 2 samples have $^{84}Kr/^{36}Ar$ ratios and $^{132}Xe/^{36}Ar$ ratios ranging from 0.069 to 0.142, and 0.0078 to 0.0098, respectively. These values ($^{84}Kr/^{36}Ar$ and $^{132}Xe/^{36}Ar$) in both groups are significantly higher than those predicted ASW values of 0.0393 and 0.00267. The mechanisms that can explain these groundwater-derived noble gas elemental fractionations and the relative enrichment of Kr and Xe are discussed in Section 5.3.

5. Discussion

5.1. Noble gas elemental compositions in the Anyue gas field

$^{4}He/^{21}Ne^{*}$ ratios in group 1 and group 2 gas samples are similar, varying from 2.17×10^{7} to 3.05×10^{7} and 2.41×10^{7} to 3.22×10^{7}, respectively. But these two groups of samples have significantly different $^{4}He/^{40}Ar^{*}$ and $^{21}Ne^{*}/^{40}Ar^{*}$ ratios as shown in Figure 9. Group 1 samples are more enriched in ^{4}He and $^{21}Ne^{*}$ compared to samples in group 2, having $^{4}He/^{40}Ar^{*}$ and $^{21}Ne^{*}/^{40}Ar^{*}$ ratios ranging from 9.15 to 10.69 and 3.37×10^{-7} to 4.22×10^{-7}, respectively (Table 3, Fig. 9). However, group 2 samples have $^{4}He/^{40}Ar^{*}$ ratios varying from 5.53 to 6.77. $^{21}Ne^{*}/^{40}Ar^{*}$ values in group 2 samples range from 1.86×10^{-7} to 2.57×10^{-7}.

Radiogenic noble gases (^{4}He, $^{21}Ne^{*}$ and $^{40}Ar^{*}$) are produced by naturally occurring radioactive elements, which accumulate in the subsurface environment over geological timescales (Ballentine and Burnard, 2002). The radiogenic production rates for ^{4}He and $^{40}Ar^{*}$ are dependent on the concentrations of the parent isotopes U/Th and K, respectively. In addition to U/Th elements, O and Mg concentrations are required for the calculation of $^{21}Ne^{*}$ production rates. No data on the concentrations of U, Th, K, O, and Mg in rocks in the Anyue gas field are available in the literature, which complicates the calculation of local radiogenic noble gas ratios. However, Kennedy et al. (1985) suggested that the correlation between $^{4}He/^{36}Ar$ and $^{40}Ar/^{36}Ar$ can be used to investigate the end member of radiogenic $^{4}He/^{40}Ar^{*}$ ratios. Correlation between $^{4}He/^{36}Ar$ and $^{40}Ar/^{36}Ar$ in Anyue gas samples enables an estimation of the local crustal radiogenic $^{4}He/^{40}Ar^{*}$ ratios in group 1 samples to be $^{4}He/^{40}Ar^{*} = 5.6$, while in group 2 samples, $^{4}He/^{40}Ar^{*} = 5.05$. Based on the local geological background, we used an average radiogenic $^{4}He/^{40}Ar^{*}$ ratio = 6 and $^{21}Ne^{*}/^{40}Ar^{*}$ ratio = 2.7×10^{-7} given by Rudnick and Fountain (1995) as the ratios of $^{4}He/^{40}Ar^{*}$ and $^{21}Ne^{*}/^{40}Ar^{*}$ in the Anyue gas field. In Fig. 9, $^{4}He/^{40}Ar^{*}$ and $^{21}Ne^{*}/^{40}Ar^{*}$ values in group 1 samples are relatively higher than the corresponding average

crustal $^{4}He/^{40}Ar^{*}$ and $^{21}Ne^{*}/^{40}Ar^{*}$ values of 6 and 2.7×10^{-7}, respectively (Rudnick and Fountain, 1995). In contrast, group 2 samples have $^{4}He/^{40}Ar^{*}$ ratios similar to the average crustal $^{4}He/^{40}Ar^{*}$ ratio of 6. But for $^{21}Ne^{*}/^{40}Ar^{*}$ values, group 2 samples are slightly lower with respect to the average crustal $^{21}Ne^{*}/^{40}Ar^{*}$ value of 2.7×10^{-7} (Rudnick and Fountain, 1995).

If radiogenic noble gases (^{4}He, $^{21}Ne^{*}$ and $^{40}Ar^{*}$) were produced in the local strata and there was little or no fractionation occurring during the migration and release processes from rock minerals, those radiogenic noble gas elemental ratios would be expected to be similar to their local production ratios governed by the average radiogenic element concentrations in the rocks along the migration pathways (Kennedy et al., 2002; Ma et al., 2009).

While radiogenic noble gases are produced and accumulated in situ in a fluid system, groundwater-derived $^{20}Ne/^{36}Ar$ ratio serves as an ideal tracer for gas migration in such a system. Therefore, radiogenic and groundwater-derived noble gases can be used together to identify the relationship of noble gases from different sources (Gilfillan et al., 2009; Hunt et al., 2012; Darrah et al., 2014; Darrah et al., 2015). Fig. 9 shows the relationships between $^{4}He/^{40}Ar^{*}$ against $^{20}Ne^{\dagger}/^{36}Ar$ and $^{21}Ne^{*}/^{40}Ar^{*}$ against $^{4}He/^{40}Ar^{*}$. In Fig.9, $^{4}He/^{40}Ar^{*}$ ratios in both group 1 and group 2 samples remain relatively stable with the increase of $^{20}Ne^{\dagger}/^{36}Ar$ ratios. The relative enrichment of ^{4}He and $^{21}Ne^{*}$ in group 1 gas samples with respect to group 2 samples is shown in Fig.9. Noble gas elemental compositions can be affected by several possible mechanisms, such as occurrence of fractionation caused by diffusive or solubility-controlled processes and thermal effect. Different mechanisms are discussed below to identify major processes that can account for the unique signature of noble gas elemental compositions between two sample groups in central Sichuan Basin.

A positive correlation between $^{21}Ne^*/^{40}Ar^*$ and $^{4}He/^{40}Ar^*$ in all samples from Anyue field has been shown in Fig. 9. Although ^{4}He and $^{21}Ne^*$ are produced by the same decay process of U and Th and yield a relatively constant $^{4}He/^{21}Ne^*$ ratio in minerals, ^{4}He could be preferentially released with respect to $^{21}Ne^*$ (Hunt et al., 2012; Darrah et al., 2014). Over time, the isotopic ratios could vary as a function of temperature, porosity, and the volume of fluid. This trend suggests that crustal noble gases may have been well mixed in the groundwater and subsequently, underwent the same fractionation in the migration process.

5.2. Mechanisms responsible for the observed noble gas elemental fractionation

5.2.1 Solubility-controlled and diffusion-controlled fractionation

Several studies have shown that in a closed gas-stripping system, $(^{20}Ne/^{36}Ar)_{sample}$ /$(^{20}Ne/^{36}Ar)_{ASW}$ values in the gas phase would start from above the ASW line and then keep going down towards the line until reaching the line $(^{20}Ne/^{36}Ar)_{sample} = (^{20}Ne/^{36}Ar)_{ASW}$ (Fig. 8) (Darrah et al., 2014; Darrah et al., 2015; Barry et al., 2016). In contrast, heavier noble gases (Kr, Xe) would start from below the ASW line and then keep going up towards the line until reaching the line $((i/^{36}Ar)_{sample} = (i/^{36}Ar)_{ASW})$ (Fig. 8). However, in an open gas-stripping system, noble gas partitioning processes would still continue after noble gas ratios in the gas phase are equal to their ASW values. As a result, gases are characterized by relatively lower $^{20}Ne/^{36}Ar$ ratios and higher $^{84}Kr/^{36}Ar$ and $^{132}Xe/^{36}Ar$ with respect to their ASW ratios at 10 °C. Therefore, the observed relatively low $^{20}Ne^{\dagger}/^{36}Ar$ ratios compared to ASW ratios at 10 °C in the Anyue field suggest the closed gas-stripping system is unlikely to apply in this study. Based on previous published work, a series of mechanisms that could explain the pattern of noble gas elemental fractionation in the Anyue gas field were modelled and tested. Two possible mechanisms were identified. Firstly, a solubility-controlled process in an open system may be responsible for groundwater-derived noble gas elemental fractionation, due to differences in

526 the solubilities of noble gases (He < Ne < Ar < Kr < Xe). Secondly, a diffusion-controlled
527 fractionation is also considered in this work as higher diffusion coefficients of He and Ne with
528 respect to Ar can lead to the relative enrichment of He and Ne during upward transport of noble
529 gases in reservoirs (Wise and Houghton, 1968; Jähne et al., 1987; Castro et al., 1998; Ma et al.,
530 2009).

531 An open system Rayleigh fractionation model is discussed below to interpret the noble
532 gas data in our samples. Rayleigh fractionation can be formulated as below:

$$\left([A]/[B]\right)_{water} = \left([A]/[B]\right)_o \times f^{(\alpha-1)} \quad (2)$$

533 Where $([A]/[B])_{water}$ is the noble gas elemental ratios in the water phase, $([A]/[B])_o$ is
534 the initial A/B ratio in the liquid (water) phase, f is the fraction of B remaining in the water
535 phase and α is the fractionation coefficient given for a gas/liquid system.

536 For solubility-controlled fractionation, α is defined as:

$$\alpha = \frac{\frac{\gamma_A}{\Phi_A} K_A^d}{\frac{\gamma_B}{\Phi_B} K_B^d} \quad (3)$$

537 Dimensionless Henry's constants K^d were derived from empiric equations (Crovetto et
538 al., 1982). Fugacity coefficient Φ and liquid activity coefficient γ were calculated following
539 Smith and Kennedy (1983) and Ballentine et al. (2002).

540 According to the gas-liquid fractionation equation given by Bosch and Mazor (1988),
541 when the gas water volume ratio (V_{gas}/V_{water}) becomes small, the noble gas elemental
542 compositions in the gas phase are fractionated proportionally to their relative solubilities in the
543 water phase:

$$\text{As } \frac{V_{gas}}{V_{water}} \to 0, \quad \frac{\left(\frac{[A]}{[B]}\right)_{gas}}{\left(\frac{[A]}{[B]}\right)_{water}} \to \frac{\frac{\gamma_A}{\Phi_A} K_A^d}{\frac{\gamma_B}{\Phi_B} K_B^d} = \alpha \tag{4}$$

The solubility-controlled Rayleigh fractionation of noble gases exsolving from the groundwater phase into the gas phase in two sample groups can be modelled using an average well depth of 3500 and 4800 m at a hydrostatic pressure of 338 and 464 atm, and a temperature of 105 and 150 °C, respectively. The salinity used in this study is 2M NaCl.

For diffusion-controlled fractionation, α is defined as:

$$\alpha_{A/B} = \sqrt{\frac{M_B}{M_A}} \tag{5}$$

where A, B denote noble gas isotopes, and M_A, M_B denote their respective mass (Marty, 1984; Jähne et al., 1987; Lippmann et al., 2003).

Average crustal $^{4}He/^{40}Ar^*$ ratio = 6 and $^{21}Ne^*/^{40}Ar^*$ ratio = 2.7×10^{-7} were chosen as the initial crustal radiogenic $^{4}He/^{40}Ar^*$ and $^{21}Ne^*/^{40}Ar^*$ ratios in the groundwater for the Rayleigh fractionation model (Ballentine and Burnard, 2002; Ozima and Podosek, 2002). The calculated ASW $^{20}Ne/^{36}Ar$ ratio for the study is 0.156. The solid red and green lines are the solubility-controlled Rayleigh fractionation model lines in the gas phase for samples in group 1 and group 2, respectively. Due to the same value of diffusion-controlled fractionation coefficient for samples in group 1 and 2, the diffusion-controlled fractionation model for samples in both groups is shown by one dashed purple line. In Fig. 9, samples in group 2 show a good fit to the solubility-controlled Rayleigh fractionation model line in the gas phase, suggesting the presence of an open system degassing of gases from the groundwater, resulting in significant noble gas elemental fractionation.

However, gas samples in group 1 are not well explained by either a gas phase solubility-controlled model or a diffusion-controlled fractionation model, as observed in Fig. 9. Although three samples are close to the diffusion-controlled $^{4}He/^{40}Ar^{*}$ and $^{21}Ne^{*}/^{40}Ar^{*}$ fractionation line, there is not enough variation in the data to be able to confidently assert that diffusive fractionation has occurred. Additionally, samples in both groups are scattered around the modelled diffusion-controlled mass fractionation lines (MFL) in a plot of $^{20}Ne/^{22}Ne$ vs. $^{38}Ar/^{36}Ar$ (not shown). Hence the possibility of a diffusion-controlled process can be ruled out as one of the main mechanisms for the observed radiogenic noble gas patterns in the two sample groups.

5.2.2 Preferential release of light noble gases from minerals

Release of radiogenic noble gases from minerals is a function of temperature (Ballentine and O'nions, 1994). For example, radiogenic ^{4}He is released from calcite at aquifer temperatures above 50 – 70 °C (Copeland et al., 2007), while the release temperature for ^{40}Ar from K-bearing feldspars is much higher at above 250 – 275 °C (Lippolt and Weigel, 1988). Although the release temperature for Ne in these minerals is uncertain, we would expect that the Ne release temperature would fall between those of He and Ar (0 – 250 °C) based on their diffusivity properties. The relative enrichment of lighter radiogenic noble gases (e.g. ^{4}He and ^{21}Ne) with respect to heavier noble gases (e.g. ^{40}Ar) in a low-temperature environment have been previously proposed by multiple researchers (Ballentine and O'nions, 1994; Darrah et al., 2014).

In this study, group 2 samples from the Cambrian formation have been buried to greater depth compared to group 1 samples in the Triassic formation. Therefore, group 1 gases have a cooler thermal history than those in group 2 samples, as evidenced by lighter $\delta^{13}C(CH_4)$ and lower C1/(C1-C5) shown in Table 1. A regime in group 1 samples, where He and Ne are preferentially released from minerals at a lower temperature than the Ar release temperature,

would explain the relative enrichment of ^{4}He and $^{21}Ne^{*}$ in group 1 gases compared to group 2 gases. This is due to hydrocarbon generation temperatures that are high enough to release ^{4}He and $^{21}Ne^{*}$, but still low enough to quantitatively retain $^{40}Ar^{*}$ (Ballentine et al., 1994). However, in group 2 samples, higher temperatures would permit more radiogenic ^{40}Ar being released from the host mineral grains over time, leading to relatively low $^{4}He/^{40}Ar^{*}$ and $^{21}Ne^{*}/^{40}Ar^{*}$ ratios.

5.3. Kr and Xe enrichment in Anyue gas field

Measured $^{84}Kr/^{36}Ar$ and $^{132}Xe/^{36}Ar$ ratios in gas samples were approximately two times and three times higher than values predicted by their respective solubility-controlled Rayleigh fractionation model (Fig.10). Two possible mechanisms may be responsible for these observed heavy noble gas enrichments. The first is gas-oil interaction and the second is the release of heavy noble gases initially trapped on source rocks.

Bosch and Mazor (1988), Kharaka and Specht (1988) and Barry et al. (2016) have shown that interaction between oil and gas can result in enrichment of heavy noble gases. However, there is no evidence of significant oil components in the Anyue gas field (Qin et al., 2018), so the involvement of oil as a mechanism for heavy noble gas enrichments is unlikely. The kerogen of the Longwangmiao formation reservoir is type I, therefore it might migrate through the oil window and interact with natural gases. Although this process cannot be discounted entirely, due to long migration distance between the source rock and reservoir in the Anyue gas field, this mechanism is not explored further. Excess heavy noble gases have also been observed in other natural gas studies. For example, similar Kr and Xe enrichments have been observed in gas reservoirs in the North Sea (Soest. et al., 2000), natural gas samples from the Sleipner Vest gas field (Barry et al., 2016) and coalbed gases from the San Juan Basin (Zhou et al., 2005). Previous work suggested that groundwater-derived heavy noble gases (Kr and Xe) can be initially adsorbed and trapped in organic-rich sediments, then escape into the

612 fluid system and mix with hydrocarbon phases, providing an additional source of these noble
613 gases. These 'additional' components have an isotopic composition indistinguishable from air
614 but lead to a relative gas abundance pattern that is highly enriched in the heavy noble gases (Kr
615 and Xe) (Torgersen and Kennedy, 1999; Kennedy et al., 2002).

616 **5.4. ^{4}He groundwater ages in the Longwangmiao formation of the Anyue gas field**

617 The accumulation of radiogenic noble gas components (e.g. ^{4}He and ^{40}Ar) in the
618 groundwater has been recognized as powerful tools to constrain the age of groundwater
619 associated with hydrocarbon reservoirs (Zhou and Ballentine, 2006; Schlegel et al., 2011; Wen
620 et al., 2015; Byrne et al., 2018a). In this study, we used ^{4}He concentrations in sample gas phase
621 in group 2 samples to derive the groundwater age information in the Longwangmiao formation
622 of the Anyue gas field.

623 **5.4.1. Calculation of initial ^{4}He concentrations in the water phase**

624 In Section 5.2, the relationship between $^{20}Ne^{\dagger}/^{36}Ar$ and $^{4}He/^{40}Ar^{*}$ in group 2 samples
625 has been interpreted as a result of open system gas loss from water following a solubility-
626 controlled Rayleigh fractionation process. Therefore, we can use solubility-controlled Rayleigh
627 fractionation model to calculate the initial ^{4}He concentrations in the water phase prior to its
628 degassing into the gas phase for each sample.

629 According to equations (2) and (4), the following equations can be derived

$$\left(^{20}Ne/^{36}Ar\right)_{water} = \left(^{20}Ne^{\dagger}/^{36}Ar\right)/\alpha_1 \quad (6)$$

$$\left(^{20}Ne/^{36}Ar\right)_{water} = \left(^{20}Ne/^{36}Ar\right)_{ASW} \times f^{\alpha_1 - 1} \quad (7)$$

630 By re-arranging (7)

$$f = \left(\left(^{20}Ne/^{36}Ar\right)_{water} / \left(^{20}Ne/^{36}Ar\right)_{ASW}\right)^{1/(\alpha_1 - 1)} \quad (8)$$

631 then using equations (4) and (2) again,

$$\left({}^{4}\mathrm{He}/{}^{36}\mathrm{Ar}\right)_{\mathrm{water}} = \left({}^{4}\mathrm{He}/{}^{36}\mathrm{Ar}\right)/\alpha_2 \quad (9)$$

$$\left({}^{4}\mathrm{He}/{}^{36}\mathrm{Ar}\right)_{\mathrm{initial}} = \left({}^{4}\mathrm{He}/{}^{36}\mathrm{Ar}\right)_{\mathrm{water}} / \left(\mathrm{f}^{\alpha_2 - 1}\right) \quad (10)$$

$$\left[{}^{4}\mathrm{He}\right]_{\mathrm{concentration\ in\ water}} = \left({}^{4}\mathrm{He}/{}^{36}\mathrm{Ar}\right)_{\mathrm{initial}} \times {}^{36}\mathrm{Ar}_{\mathrm{ASW}} \quad (11)$$

where $\alpha_1$and α_2 denote the fractionation coefficients of $^{20}Ne/^{36}Ar$ and $^{4}He/^{36}Ar$ given for a gas/liquid system, respectively. The calculated solubility-controlled fractionation coefficients α_1 and α_2 using equation (3) in group 2 samples are 1.4681 and 1.3194, respectively. $^{36}Ar_{ASW}$ represents the concentration of ^{36}Ar in equilibrium with water which depends on elevation, temperature and salinity of the water during recharge at the surface. An average Ar concentration of 7.56×10^{-7} $cm^3STPg^{-1}_{H2O}$ is taken as a representative $^{36}Ar_{ASW}$ value calculated at 10 °C at an altitude of 400 m, i.e., the mean annual air temperature and average altitude in central Sichuan Basin (Stute et al., 1992; Stute et al., 1995; Kipfer et al., 2002; Liu et al., 2012). The initial $^{20}Ne/^{36}Ar$ ratio in the water $^{20}Ne/^{36}Ar_{ASW}$ is calculated as 0.156.

The calculated initial ^{4}He concentrations in the water phase in Longwangmiao reservoir range from 6.41×10^{-3} to 2.23×10^{-2} cm^3STP/cm^3 H_2O (Table 4).

5.4.2. ^{4}He groundwater ages in closed and open systems

The determination of ^{4}He ages for groundwater associated with hydrocarbon systems followed the method in Zhou and Ballentine (2006). Since mantle He is negligible in our study area as discussed previously, the measured ^{4}He in the groundwater can be derived from three different sources: atmospheric ^{4}He in air saturated water, ^{4}He obtained from radioactive decay of primarily U and Th in the aquifer matrix (in-situ production) and ^{4}He originated from older crustal fluids that has migrated into the aquifer (external flux). The ^{4}He /^{20}Ne ratios in all samples are much higher than the atmospheric value of $^{4}He/^{20}Ne$ = 0.288, indicating that the atmospheric He contributions are negligible. Therefore, the amount of ^{4}He in the groundwater system can be expressed as:

$$^4\mathrm{He}_{\mathrm{measured}} = {}^4\mathrm{He}_{\mathrm{in\ situ\ production}} + {}^4\mathrm{He}_{\mathrm{external\ flux}} \quad (12)$$

653 The in-situ production of ^{4}He can be expressed as (Torgersen, 1980):

$$\left[{}^4\mathrm{He}\right]_{\mathrm{in\ situ\ production}} = \frac{\rho \Lambda J_4 (1-\varphi)}{\varphi} t \quad (13)$$

654 where $\rho_{aquifer}$ denotes the density of the aquifer (g/cm^3), Λ is transfer efficiency from
655 mineral to water, which is assumed to be 1 (Torgersen, 1980; Torgersen and Clarke, 1985), φ
656 denotes rock porosity, t denotes groundwater residence time, and J_4 is defined by:

$$J_4 = 0.2355 \times 10^{-12} \times [U] \times \left(1 + 0.123 \times \left([Th]/[U] - 4\right)\right) \quad (14)$$

657 where $[U]$ and $[Th]$ are the U and Th concentrations in the rock in ppm (Craig and
658 Lupton, 1976; Torgersen, 1980).

659 $^4\mathrm{He}_{\mathrm{external\ flux}}$ can be calculated by

$$\left[{}^4\mathrm{He}\right]_{\mathrm{external\ flux}} = \frac{F_4}{\varphi h} t \quad (15)$$

$$F_4 = J_4 \times \rho \times H \quad (16)$$

660
661 where F_4 represents the average external crustal ^{4}He flux in cm^3 STP ^{4}He/cm$^2_{\mathrm{rock}}$ year,
662 ρ_{crust} denotes the crust density, H denotes the crust thickness (cm), and h denotes the aquifer
663 thickness (cm).

664

665 ^{4}He groundwater ages are calculated for both closed system and open system scenarios.
666 In a closed system, only ^{4}He produced in-situ is considered to have accumulated in
667 groundwater over geological time, while in an open system, in addition to in-situ produced ^{4}He,
668 an average external ^{4}He flux has been included, which is introduced from deep crust into the
669 groundwater system. By using parameter values shown in Table 5 and assuming a closed
670 system, the calculated ^{4}He groundwater ages of group 2 samples from the Anyue gas field

range from 280 to 974 Ma (Fig. 11). Some of these ages are older than the deposition of the reservoir rocks, implying an external flux, which has been shown to play a significant role in the determination of groundwater ^{4}He ages (Zhou and Ballentine, 2006; Schlegel et al., 2011; Wen et al., 2015). Therefore, we consider ^{4}He accumulation from external sources when determining the age of associated groundwater. If an external flux of ^{4}He from the crust (open system) is assumed (See equations 15 and16), the groundwater ^{4}He ages decrease to 1.10 - 3.84 Ma in the Longwangmiao formation of the Anyue gas field. Therefore, the calculated open system groundwater ages are significantly younger than those in their formation ages, indicating that there is no significant preservation of ^{4}He from formation water. Significant difference between the groundwater ^{4}He ages calculated for closed and open systems suggests that large amount of external crustal flux of ^{4}He have contributed to the accumulation of ^{4}He in the groundwater in the Longwangmiao formation of the Anyue gas field.

5.5 Gas and groundwater volume ratio

Groundwater-derived noble gases (e.g. ^{20}Ne, ^{36}Ar, ^{84}Kr and ^{132}Xe) can be introduced into hydrocarbon systems during the interaction with air saturated groundwater. Due to their low solubilities, noble gases preferentially partition into the hydrocarbon phase according to Henry's law, which is referred to as 'gas stripping' process. Therefore, we can utilize noble gas concentrations and elemental ratios to quantify the extent of hydrocarbon-water exchange (e.g. gas/water ratios), which places important constraints on water interaction with hydrocarbons, as well as hydrocarbon migration histories, storage mechanisms and reservoir conditions over geological timescale (Ballentine et al., 1991; Ballentine et al., 1996; Torgersen and Kennedy, 1999; Zhou et al., 2005; Darrah et al., 2014; Darrah et al., 2015; Barry et al., 2016; Barry et al., 2017). This information is also useful for the assessment of viable hydrocarbon exploration by the industries.

695 The noble gas constrained gas/water volume ratios (V_g/V_w) were calculated following
696 the open system degassing model described in Barry et al. (2016). The reservoir conditions
697 (reservoir pressure = 470.15 bar, reservoir temperature = 423.15 K and salinity = 2 M) and
698 groundwater recharge conditions (recharge temperature = 283.15 K) were used for V_g/V_w ratio
699 calculation in the Longwangmiao formation of the Anyue gas field. It is assumed that
700 hydrocarbons are initially devoid of air-derived noble gases, and they are acquired only during
701 gas-water exchange (Bosch and Mazor, 1988; Barry et al., 2016; Barry et al., 2017).

$$\frac{V_g}{V_w} = \frac{G}{W}\left(\frac{ln\left(\frac{\left(\frac{^{20}Ne^{\dagger}}{^{36}Ar}\right)_{meas}}{\left[\frac{K^{M}_{^{20}Ne}}{K^{M}_{^{36}Ar}}\right]\left(\frac{^{20}Ne}{^{36}Ar}\right)_{ASW}} \right)}{ln\left(\frac{F_{^{20}Ne}}{F_{^{36}Ar}}\right)} \right) \quad (17)$$

702

$$F = \frac{\left(\frac{22400 T_R \rho_W}{1000 \times 273.15\ K_i^M}\right)}{\left(\frac{22400 T_R \rho_W}{1000 \times 273.15\ K_i^M}\right) + \frac{G}{W}} \quad (18)$$

703

704 where F is the term that describes the relative partitioning between an assumed volume
705 of gas 'G' and water packet 'W'(Barry et al., 2016). T_R is the reservoir temperature (K), ρ_w is
706 the density of water and K_i^M is the reservoir temperature and salinity specific Henry's constant
707 (Crovetto et al., 1982; Smith and Kennedy, 1983).

708 The noble gas estimate of volumetric gas/water ratios (V_g/V_w) in the Longwangmiao
709 formation of the Anyue gas field range from 0.020 to 0.073, with an average value of 0.041 at
710 reservoir temperature and pressure (RTP). The dilution factor F, which constrains the extent of

groundwater associated CH_4, can be expressed as measured air-corrected ^{20}Ne concentration ($^{20}Ne^{\dagger}$) over Rayleigh fractionation modelled ^{20}Ne concentration, ranging from 4.31×10^{-4} to 1.76×10^{-3}.

$$F = \frac{C_{^{20}Ne^{\dagger}}}{C_{\text{model}\,^{20}Ne}} \tag{19}$$

The Longwangmiao formation gas reservoir has been proven to be the largest integrated carbonate gas reservoir in China, with an estimated gas reserve of 4404×10^8 m^3STP (Ma, 2016). Based on an average dilution ratio of 8.3×10^{-4} in the study area, the calculated volume of gases that interacted with groundwater is 1.2×10^{-3} km^3 at RTP. Therefore, by using the average V_g/V_w value and calculated gas volumes, the volume of the associated water is predicted to be 0.030 km^3. The ratio of groundwater volume involved in the gas production to the estimated total gas reserves is 0.020 km^3H_2O/km^3(gas) at reservoir temperature and pressure. Therefore, only a small fraction of the gas in the reservoir has interacted with groundwater according to noble gas data.

5.6 Gas and groundwater interaction indicated by $CH_4/^{36}Ar$ ratio

CH_4 is the most dominant natural gas in the Anyue gas field, and the solubility of gas in water depends on temperature, pressure and water salinity (Price et al., 1981; Ballentine et al., 1991). Although the solubilities of CH_4 and ^{36}Ar are not available at greater depth, the $CH_4/^{36}Ar$ ratio in water should be constant due to their similar solubilities. In order to further understand the role of groundwater in the origin, accumulation and transportation of natural gases, we modelled $CH_4/^{36}Ar$ ratios as a function of depth in CH_4 saturated pure water and 2M NaCl saline water based on the data from Ballentine et al. (1991). The green and red dotted lines in Fig. 12 show expected $CH_4/^{36}Ar$ ratios for the CH_4 saturated pure water and 2M NaCl saline water, respectively. Due to similar solubilities of CH_4 and ^{36}Ar in water, the $CH_4/^{36}Ar$

ratios in any gas phase previously exsolved from groundwater should not deviate significantly from the initial dissolved $CH_4/^{36}Ar$ ratio (Ballentine et al., 1991). Due to lack of exact depth data in this study, depth values (5 wells) from Liu et al. (2015) were used to make a plot of measured $CH_4/^{36}Ar$ ratios in the Anyue gas field as a function of depth. The measured $CH_4/^{36}Ar$ ratios in five gas samples range from 116×10^6 to 230×10^6, showing a significant deviation from expected $CH_4/^{36}Ar$ ratios in the CH_4 saturated pure water and 2M NaCl saline water. This additional evidence suggests that the majority of natural gases in Anyue gas field did not interact with the young groundwater system currently in contact with the gas reservoir.

5.7 The role of groundwater in gas preservation and accumulation in the Anyue field

The Sichuan Basin has experienced continuous burial and high-thermal evolution during the Permian-Late Cretaceous with large amount of gases being generated, resulting in abnormally high temperature and pressure in Sinian-Cambrian paleo-reservoirs (Ma et al., 2008; Yuan et al., 2012; Wei et al., 2014). Later, the occurrence of tectonic movement during the Himalayan period caused significant uplift of the central Sichuan Basin with overlying formations denudated (Fig. 2). Due to a dramatic decrease in temperature and pressure in the subsurface environment, natural gas that was previously dissolved in the formation water could exsolve and form a free gas phase in structural highs or migrate into existing gas reservoirs (Yuan et al., 2012; Qin et al., 2018).

Less negative $\delta^{13}C(CH_4)$ values in free gas samples than those in bitumen samples (Fig.4) can be explained by considering the geological history of the Anyue gas field. As both free gas and bitumen samples are from the same formation (Longwangmiao formation) of the Anyue gas field, assuming $\delta^{13}C$ values in gases originally generated from the same source as the reservoir bitumen were more negative than those in the bitumen samples, when gases dissolved into groundwater, $\delta^{13}C$ values in the dissolved gases could be elevated and became

759 less negative than those in the bitumen samples. This mechanism is also supported by the stable
760 carbon isotope $\delta^{13}C$ values in current water-dissolved gases which are less negative than those
761 in the free gas samples. However, noble gas data in the Longwangmiao formation of the Anyue
762 gas field suggested that there was only a limited amount of young groundwater, during basin
763 geological history, that was in contact with the gases in the reservoir. Stable carbon isotopic
764 fractionation pattern in all samples suggested that the possibility of only one stage gas and
765 groundwater interaction in the reservoir can be excluded.

766 Based on the stable carbon isotope pattern in the free gas, water-dissolved gas and
767 reservoir bitumen and noble gas derived gas groundwater interaction models, we suggest there
768 was a two-stage gas groundwater interaction in the gas preservation and accumulation history
769 in the Longwangmiao formation of the Anyue gas field. In the first stage, large amount of gases
770 generated during Permian-Late Cretaceous was dissolved into groundwater. This interaction
771 elevated the carbon isotope $\delta^{13}C$ values in the water-dissolved gas to be higher than those in
772 the reservoir bitumen. Due to low solubilities of noble gases and the existence of large amounts
773 of gases generated in this period, all noble gases in the original formation water had been
774 stripped from the water phase. During the Himalayan tectonic plate movement (40 – 50Ma),
775 Sichuan Basin was uplifted and most hydrocarbon gases together with noble gases have been
776 lost due to lack of a stable trapping structure. The noble gas contents in the original formation
777 water were lost completely during this period. Although mixing between gases from different
778 sources and thermal maturities could elevate $\delta^{13}C(CH_4)$ values and cause isotopic reversal
779 between methane and ethane in unconventional reservoirs (Burruss and Laughrey, 2010; Hunt
780 et al., 2012), Anyue gas field is a conventional field and there is no observed isotopic reversal
781 among gases. This mechanism to elevate $\delta^{13}C$ (CH_4) values can therefore be excluded. In
782 addition, a recent study by Leonte et al. (2018) suggested that $\delta^{13}C(CH_4)$ values could be
783 modified significantly while gas bubbles were going through a water column. This isotopic

784 effect has been demonstrated both in samples collected from a field experiment and theoretical
785 modelling.

786 The gases accumulated in the current reservoir are mainly from gases exsolved from
787 the original formation water with observed elevated stable carbon $\delta^{13}C(CH_4)$ values higher
788 than reservoir bitumen samples. Later on, relatively young meteoric groundwater (~3 Ma)
789 contacted the gases which were trapped in the current reservoir. The noble gases from the
790 second stage of the gas and groundwater interaction have been preserved in the reservoir since
791 that time. However, based on the noble gas-constrained gas/water volume ratios and measured
792 $CH_4/^{36}Ar$ ratios in samples as discussed in the previous section, there was only a small fraction
793 of gases in the reservoir were in contact with groundwater. The second stage gas and
794 groundwater interaction further elevated the stable carbon $\delta^{13}C$ values in the gases dissolved
795 in the young groundwater, as demonstrated by the $\delta^{13}C$ values in the gases in the water samples
796 from the Anyue gas field (Fig. 4). This two-stage gas and groundwater interaction model is
797 illustrated in a schematic diagram in Fig. 13. Several studies have also reported that the
798 formation of some giant gas fields was associated with release and accumulation of gases
799 previously dissolved in groundwater, such as the Urengoy gas field in the west Siberia Basin
800 and the Hetianhe gas field in the Tarim Basin, NW China (Littke et al., 2001; Cramer et al.,
801 2002; Qin et al., 2006; Yuan et al., 2012).
802

803 **6. Conclusions**

804 In this paper, we present noble gas and stable carbon isotope data for thirteen natural
805 gas, five reservoir bitumen and nine formation water samples from the Anyue gas field in the
806 central Sichuan Basin, China. Major gas composition data show that CH_4 is the dominant gas
807 in the gas samples, with a dryness coefficient (C_1/C_1-C_5) of up to 0.9996. Natural gases in the
808 study area are of thermogenic origin with $\delta^{13}C(CH_4)$ isotopes ranging from -35.0 to -34.6 ‰,

809 and -34.2 to -32.6 ‰ in group 1 and group 2 samples, respectively. The pattern of $\delta^{13}C$ values
810 among three different types of samples suggests strong gas and groundwater interaction in the
811 Longwangmiao formation of the Anyue gas field.

812 Noble gas data show that $^{3}He/^{4}He$ (R/R_a) values measured in samples from the Anyue
813 gas field range from 0.0118 to 0.0256, indicating the absence of a mantle source. $^{20}Ne/^{22}Ne$
814 and $^{21}Ne/^{22}Ne$ ratios suggest a mixing of the air and crust sources. $^{40}Ar/^{36}Ar$ ratios in all samples
815 are significantly higher than the air value of 298.6. Heavier noble gas isotopes (Kr and Xe) are
816 predominantly air-like. Samples in group 1 are relatively more enriched in ^{4}He and $^{21}Ne^{*}$. This
817 can be explained by preferential release of He and Ne relative to Ar from minerals at low
818 temperatures. In contrast, the noble gas isotopic ratios for samples in group 2 are significantly
819 altered by an open system solubility-controlled Rayleigh fractionation mechanism. Excess
820 heavy noble gases (Kr and Xe) in natural gas samples indicates the release of sedimentary
821 components from source rocks during geological evolution. In order to better constrain the role
822 of water in the Anyue gas field as well as the extent of interactions between gas and
823 groundwater, groundwater ages were calculated using ^{4}He accumulated in gas samples. The
824 gas/groundwater volume ratios were also derived for sampled wells in the Anyue gas field. ^{4}He
825 groundwater ages in the Longwangmiao formation of the Anyue gas field indicate that
826 relatively young groundwater, compared to the gas formation history, has been introduced into
827 the gas trapping structure. However, the noble gas constrained volumetric gas/groundwater
828 ratios (V_g/V_w) in the Anyue gas field vary from 0.020 to 0.073 at reservoir temperature and
829 pressure (RTP), indicating that only a small amount of gases in the reservoir has interacted
830 with the young groundwater. In addition, measured $CH_4/^{36}Ar$ ratios significantly deviate from
831 expected $CH_4/^{36}Ar$ ratios in the CH_4 saturated pure water and 2M NaCl saline water, which
832 suggests that natural gases in the Anyue gas field are unlikely derived from the current

833 groundwater system. The gas reservoir in the study area has formed prior to interaction with
834 current groundwater.

835 We propose a two-stage gas and groundwater interaction during the preservation and
836 accumulation of the gases in the Anyue gas field. The majority of the gases currently trapped
837 in the Anyue reservoir are derived from gases dissolved in the original formation water.
838 Continuous tectonic uplifting movements during the Himalayan period induced the release of
839 previously dissolved natural gases into the free gas phase in structural highs or gases migrated
840 into existing gas reservoirs due to the significant decrease in temperature and pressure in the
841 reservoir. Later, meteoric water recharge caused a relatively young groundwater system to
842 come into contact with the gases in the reservoir. Studies on gas-groundwater interactions in
843 the subsurface environment can not only provide better understanding of the role groundwater
844 plays in gas accumulation, but also provide new insights on future hydrocarbon investigation
845 and exploration.

846

847 **Acknowledgements**

848 YL acknowledges China Scholarship Council for financial support. This research has been
849 funded by Natural Environment Research Council of UK (Grant Ref: NE/T004452/1), National
850 Natural Science Foundation of China (Grant No. 41872162), Chinese Academy of Sciences
851 (Grant No. XDA14010103), China National Major S&T Program (Grant No. 2017ZX05008-
852 002-030) and State Key Laboratory of Organic Geochemistry (Grant No. SKLOG201842). We
853 thank operators at PetroChina for sampling assistance. We especially thank Dave Hughes for
854 the assistance in laboratory. This work has benefitted from discussion with Dr. Wen Zhang.
855 Helpful comments from Dr. Huanfang Huang are appreciated. We thank Paul Mclachlan and
856 Mounir Takriti for language correction. Comments from associate editor Dr. Chris Hall,
857 reviewer Dr. Tom Darrah and two anonymous reviewers have greatly improved this manuscript.

Research Data

Research Data associated with this article can be access at http://dx.doi.org/10.17632/33hzcsyc6k.3

References

Ballentine, C.J., Burgess, R. and Marty, B. (2002) Tracing Fluid Origin, Transport and Interaction in the Crust. *Rev.Mineral.Geochem.* **47**, 539-614.

Ballentine, C.J. and Burnard, P.G. (2002) Production, Release and Transport of Noble Gases in the Continental Crust. *Reviews in Mineralogy and Geochemistry* **47**, 481-538.

Ballentine, C.J., Mazurek, M. and Gautschi, A. (1994) Thermal constraints on crustal rare gas release and migration: Evidence from Alpine fluid inclusions. *Geochim. Cosmochim. Ac.* **58**, 4333-4348.

Ballentine, C.J., O'Nions, R.K. and Coleman, M.L. (1996) A Magnus opus: Helium, neon, and argon isotopes in a North Sea oilfield. *Geochim. Cosmochim. Ac.* **60**, 831-849.

Ballentine, C.J. and O'nions, R.K. (1994) The use of natural He, Ne and Ar isotopes to study hydrocarbon-related fluid provenance, migration and mass balance in sedimentary basins. *Geol. Soc., Lond., Spec. Publ.* **78**, 347-361.

Ballentine, C.J., Onions, R.K., Oxburgh, E.R., Horvath, F. and Deak, J. (1991) Rare-Gas Constraints on Hydrocarbon Accumulation, Crustal Degassing and Groundwater-Flow in the Pannonian Basin. *Earth Planet. Sci. Lett.* **105**, 229-246.

Ballentine, C.J. and Sherwood Lollar, B. (2002) Regional groundwater focusing of nitrogen and noble gases into the Hugoton-Panhandle giant gas field, USA. *Geochim. Cosmochim. Ac.* **66**, 2483-2497.

Barry, P.H., Kulongoski, J.T., Landon, M.K., Tyne, R.L., Gillespie, J.M., Stephens, M.J., Hillegonds, D.J., Byrne, D.J. and Ballentine, C.J. (2018) Tracing enhanced oil recovery signatures in casing gases from the Lost Hills oil field using noble gases. *Earth Planet. Sci. Lett.* **496**, 57-67.

Barry, P.H., Lawson, M., Meurer, W.P., Danabalan, D., Byrne, D.J., Mabry, J.C. and Ballentine, C.J. (2017) Determining fluid migration and isolation times in multiphase crustal domains using noble gases. *Geology* **45**, 775-778.

Barry, P.H., Lawson, M., Meurer, W.P., Warr, O., Mabry, J.C., Byrne, D.J. and Ballentine, C.J. (2016) Noble gases solubility models of hydrocarbon charge mechanism in the Sleipner Vest gas field. *Geochim. Cosmochim. Ac.* **194**, 291-309.

Battani, A., Sarda, P. and Prinzhofer, A. (2000) Basin scale natural gas source, migration and trapping traced by noble gases and major elements: the Pakistan Indus basin. *Earth Planet. Sci. Lett.* **181**, 229-249.

Bosch, A. and Mazor, E. (1988) Natural gas association with water and oil as depicted by atmospheric noble gases: case studies from the southeastern Mediterranean Coastal Plain. *Earth Planet. Sci. Lett.* **87**, 338-346.

Burruss, R.C. and Laughrey, C.D. (2010) Carbon and hydrogen isotopic reversals in deep basin gas: Evidence for limits to the stability of hydrocarbons. *Org. Geochem.* **41**, 1285-1296.

Byrne, D.J., Barry, P.H., Lawson, M. and Ballentine, C.J. (2018a) Determining gas expulsion vs retention during hydrocarbon generation in the Eagle Ford Shale using noble gases. *Geochim. Cosmochim. Ac.* **241**, 240-254.
Byrne, D.J., Barry, P.H., Lawson, M. and Ballentine, C.J. (2018b) Noble gases in conventional and unconventional petroleum systems. *Geol. Soc., Lond., Spec. Publ.* **468**, 127-149.
Cai, C., Worden, R.H., Bottrell, S.H., Wang, L. and Yang, C. (2003) Thermochemical sulphate reduction and the generation of hydrogen sulphide and thiols (mercaptans) in Triassic carbonate reservoirs from the Sichuan Basin, China. *Chem. Geol.* **202**, 39-57.
Cao, C., Zhang, M., Tang, Q., Yang, Y., Lv, Z., Zhang, T., Chen, C., Yang, H. and Li, L. (2018) Noble gas isotopic variations and geological implication of Longmaxi shale gas in Sichuan Basin, China. *Mar. Petrol. Geol.* **89**, 38-46.
Castro, M.C., Jambon, A., Marsily, G. and Schlosser, P. (1998) Noble gases as natural tracers of water circulation in the Paris Basin: 1. Measurements and discussion of their origin and mechanisms of vertical transport in the basin. *Water Resour. Res.* **34**, 2443-2466.
Chen, Z., Yang, Y., Wang, T.G., Cheng, B., Li, M., Luo, B., Chen, Y., Ni, Z., Yang, C., Chen, T., Fang, R. and Wang, M. (2017) Dibenzothiophenes in solid bitumens: Use of molecular markers to trace paleo-oil filling orientations in the Lower Cambrian reservoir of the Moxi–Gaoshiti Bulge, Sichuan Basin, southern China. *Org. Geochem.* **108**, 94-112.
Colwell, F.S., Onstott, T.C., Delwiche, M.E., Chandler, D., Fredrickson, J.K., Yao, Q.J., McKinley, J.P., Boone, D.R., Griffiths, R., Phelps, T.J., Ringelberg, D., White, D.C., LaFreniere, L., Balkwill, D., Lehman, R.M., Konisky, J. and Long, P.E. (1997) Microorganisms from deep, high temperature sandstones: constraints on microbial colonization. *FEMS Microbiol. Rev.* **20**, 425-435.
Copeland, P., Watson, E.B., Urizar, S.C., Patterson, D. and Lapen, T.J. (2007) Alpha thermochronology of carbonates. *Geochim. Cosmochim. Ac.* **71**, 4488-4511.
Craig, H. and Lupton, J.E. (1976) Primordial neon, helium, and hydrogen in oceanic basalts. *Earth Planet. Sci. Lett.* **31**, 369-385.
Cramer, B., Schlömer, S. and Poelchau, H.S. (2002) Uplift-related hydrocarbon accumulations: the release of natural gas from groundwater. *Geol. Soc., Lond., Spec. Publ.* **196**, 447.
Crovetto, R., Fernández-Prini, R. and Japas, M.L. (1982) Solubilities of inert gases and methane in H2O and in D2O in the temperature range of 300 to 600 K. *J. Chem. Phys.* **76**, 1077-1086.
Dai, J., Pei, X. and Qi, H. (1992) Natural Gas Geology in China. *Petroleum Industry Press, Beijing* **1**, 102-104 (in Chinese).
Dai, J., Song, Y. and Zhang, H. (1997) Main factors controlling the foundation of medium-giant gas fields in China. *Science in China Series D: Earth Sciences* **40**, 1-10.
Dai, J., Zou, C., Liao, S., Dong, D., Ni, Y., Huang, J., Wu, W., Gong, D., Huang, S. and Hu, G. (2014) Geochemistry of the extremely high thermal maturity Longmaxi shale gas, southern Sichuan Basin. *Org. Geochem.* **74**, 3-12.
Dai, J.X., Ni, Y.Y. and Zou, C.N. (2012) Stable carbon and hydrogen isotopes of natural gases sourced from the Xujiahe Formation in the Sichuan Basin, China. *Org. Geochem.* **43**, 103-111.
Darrah, T.H., Jackson, R.B., Vengosh, A., Warner, N.R., Whyte, C.J., Walsh, T.B., Kondash, A.J. and Poreda, R.J. (2015) The evolution of Devonian hydrocarbon gases in shallow aquifers of the northern Appalachian Basin: Insights from integrating noble gas and hydrocarbon geochemistry. *Geochim. Cosmochim. Ac.* **170**, 321-355.
Darrah, T.H., Vengosh, A., Jackson, R.B., Warner, N.R. and Poreda, R.J. (2014) Noble gases identify the mechanisms of fugitive gas contamination in drinking-water wells overlying the

Marcellus and Barnett Shales. *Proceedings of the National Academy of Sciences* **111**, 14076-14081.
Ding, X., Wang, B., Wang, X., Liu, H., Zeng, D. and Feng, M. (2018) The three different types of paleokarstification and reservoir distribution of Leikoupo Formation, Middle Triassic in the northern Sichuan Basin, China. *Carbonates and Evaporites* **33**, 243-254.
Dow, W.G. (1977) Kerogen studies and geological interpretations. *J. Geochem. Explor.* **7**, 79-99.
Du, J., Zou, C., Xu, C., He, H., Shen, P., Yang, Y., Li, Y., Wei, G., Wang, Z. and Yang, Y. (2014) Theoretical and technical innovations in strategic discovery of a giant gas field in Cambrian Longwangmiao Formation of central Sichuan paleo-uplift, Sichuan Basin. *Petrol. Explor. Dev.* **41**, 294-305.
Dunai, T.J. and Porcelli, D. (2002) Storage and Transport of Noble Gases in the Subcontinental Lithosphere. *Rev.Mineral.Geochem.* **47**, 371-409.
Fetter, N., Blichert-Toft, J., Télouk, P. and Albarède, F. (2019) Extraction of Pb and Zn from crude oil for high-precision isotopic analysis by MC-ICP-MS. *Chem. Geol.* **511**, 112-122.
Gilfillan, S.M., Lollar, B.S., Holland, G., Blagburn, D., Stevens, S., Schoell, M., Cassidy, M., Ding, Z., Zhou, Z., Lacrampe-Couloume, G. and Ballentine, C.J. (2009) Solubility trapping in formation water as dominant CO(2) sink in natural gas fields. *Nature* **458**, 614-618.
Hao, F., Guo, T., Zhu, Y., Cai, X., Zou, H. and Li, P. (2008) Evidence for multiple stages of oil cracking and thermochemical sulfate reduction in the Puguang gas field, Sichuan Basin, China. *AAPG Bull.* **92**, 611-637.
Holland, G. and Ballentine, C.J. (2006) Seawater subduction controls the heavy noble gas composition of the mantle. *Nature* **441**, 186-191.
Huang, J., Chen, S., Song, J., Wang, L., Gou, X., Wang, T. and Dai, H. (1997) Hydrocarbon source systems and formation of gas fields in Sichuan Basin. *Science in China Series D: Earth Sciences* **40**, 32-42.
Hunt, A.G., Darrah, T.H. and Poreda, R.J. (2012) Determining the source and genetic fingerprint of natural gases using noble gas geochemistry: A northern Appalachian Basin case study. *AAPG Bull.* **96**, 1785-1811.
Jähne, B., Heinz, G. and Dietrich, W. (1987) Measurement of the diffusion coefficients of sparingly soluble gases in water. *J. Geophys. Res. Oceans* **92**, 10767-10776.
Jiang, L., Hu, S., Zhao, W., Xu, Z., Shi, S., Fu, Q., Zeng, H., Liu, W. and Fall, A. (2018) Diagenesis and its impact on a microbially derived carbonate reservoir from the Middle Triassic Leikoupo Formation, Sichuan Basin, China. *AAPG Bull.* **102**, 2599-2628.
Jin, X., Pan, C., Yu, S., Li, E., Wang, J., Fu, X., Qin, J., Xie, Z., Zheng, P., Wang, L., Chen, J. and Tan, Y. (2014) Organic geochemistry of marine source rocks and pyrobitumen-containing reservoir rocks of the Sichuan Basin and neighbouring areas, SW China. *Mar. Petrol. Geol.* **56**, 147-165.
Kennedy, B.M., Lynch, M.A., Reynolds, J.H. and Smith, S.P. (1985) Intensive sampling of noble gases in fluids at Yellowstone: I. Early overview of the data; regional patterns. *Geochim. Cosmochim. Ac.* **49**, 1251-1261.
Kennedy, B.M., Torgersen, T. and van Soest, M.C. (2002) Multiple atmospheric noble gas components in hydrocarbon reservoirs: a study of the Northwest Shelf, Delaware Basin, SE New Mexico. *Geochim. Cosmochim. Ac.* **66**, 2807-2822.
Kharaka, Y.K. and Specht, D.J. (1988) The solubility of noble gases in crude oil at 25–100°C. *Appl. Geochem.* **3**, 137-144.
Kipfer, R., Aeschbach-Hertig, W., Peeters, F. and Stute, M. (2002) Noble Gases in Lakes and Ground Waters. *Rev.Mineral.Geochem.* **47**, 615-700.

Larter, S.R., Bowler, B.F.J., Li, M., Chen, M., Brincat, D., Bennett, B., Noke, K., Donohoe, P., Simmons, D., Kohnen, M., Allan, J., Telnaes, N. and Horstad, I. (1996) Molecular indicators of secondary oil migration distances. *Nature* **383**, 593-597.
Le, L. (2015) Study on sedimentary environment and origin of analcime-bearing dolomite of shahejie formation in Tanggu area. China University of Geosciences, China University of Geosciences.
Lee, J.Y., Marti, K., Severinghaus, J.P., Kawamura, K., Yoo, H.-S., Lee, J.B. and Kim, J.S. (2006) A redetermination of the isotopic abundances of atmospheric Ar. *Geochim. Cosmochim. Ac.* **70**, 4507-4512.
Leonte, M., Wang, B., Socolofsky, S.A., Mau, S., Breier, J.A. and Kessler, J.D. (2018) Using Carbon Isotope Fractionation to Constrain the Extent of Methane Dissolution Into the Water Column Surrounding a Natural Hydrocarbon Gas Seep in the Northern Gulf of Mexico. *Geochem. Geophys. Geosyst.* **19**, 4459-4475.
Li, J., Xie, Z.Y., Dai, J.X., Zhang, S.C., Zhu, G.Y. and Liu, Z.L. (2005) Geochemistry and origin of sour gas accumulations in the northeastern Sichuan Basin, SW China. *Org. Geochem.* **36**, 1703-1716.
Li, P.P., Hao, F., Guo, X.S., Zou, H.Y., Yu, X.Y. and Wang, G.W. (2015) Processes involved in the origin and accumulation of hydrocarbon gases in the Yuanba gas field, Sichuan Basin, southwest China. *Mar. Petrol. Geol.* **59**, 150-165.
Li, Y. (2019) Tracing fluid dynamics with noble gas and stable isotope systematics: examples from Krafla, Iceland and Sichuan Basin, China. Lancaster University, p. 169.
Li, Y.J., Feng, Y.Y., Liu, H., Zhang, L.H. and Zhao, S.X. (2013) Geological characteristics and resource potential of lacustrine shale gas in the Sichuan Basin, SW China. *Petrol. Explor. Dev.* **40**, 454-460.
Liang, C., Jiang, Z.X., Zhang, C.M., Guo, L., Yang, Y.T. and Li, J. (2014) The shale characteristics and shale gas exploration prospects of the Lower Silurian Longmaxi shale, Sichuan Basin, South China. *J. Nat. Gas Sci. Eng.* **21**, 636-648.
Lippmann, J., Stute, M., Torgersen, T., Moser, D.P., Hall, J.A., Lin, L., Borcsik, M., Bellamy, R.E.S. and Onstott, T.C. (2003) Dating ultra-deep mine waters with noble gases and 36Cl, Witwatersrand Basin, South Africa. *Geochim. Cosmochim. Ac.* **67**, 4597-4619.
Lippolt, H.J. and Weigel, E. (1988) 4He diffusion in 40Ar-retentive minerals. *Geochim. Cosmochim. Ac.* **52**, 1449-1458.
Littke, R., Cramer, B., Gerling, P., Lopatin, N.V., Poelchau, H.S., Schaefer, R.G. and Welte, D.H. (2001) Gas Generation and Accumulation in the West Siberian Basin: Reply. *AAPG Bull.* **85**, 1893-1895.
Liu, S., Deng, B., Li, Z. and Sun, W. (2012) Architecture of basin-mountain systems and their influences on gas distribution: A case study from the Sichuan basin, South China. *J. Asian Earth Sci.* **47**, 204-215.
Liu, Y., Zheng, L., Qiu, N., Jia, J. and Chang, Q. (2015) The Effect of Temperature on the Overpressure Distribution and Formation in the Central Paleo-Uplift of the Sichuan Basin. *Chinese J. Geophys.* **58**, 340-351.
Lollar, B.S., O'Nions, R.K. and Ballentine, C.J. (1994) Helium and neon isotope systematics in carbon dioxide-rich and hydrocarbon-rich gas reservoirs. *Geochim. Cosmochim. Ac.* **58**, 5279-5290.
Ma, L., Castro, M.C. and Hall, C.M. (2009) Crustal noble gases in deep brines as natural tracers of vertical transport processes in the Michigan Basin. *Geochem. Geophys. Geosyst.* **10**, 1-24.
Ma, X. (2016) Innovation-driven efficient development of the Longwangmiao Fm large-scale sulfur gas reservoir in Moxi block, Sichuan Basin. *Nat. Gas Ind.* **3**, 99-107.

Ma, Y.S., Zhang, S.C., Guo, T.L., Zhu, G.Y., Cai, X.Y. and Li, M.W. (2008) Petroleum geology of the Puguang sour gas field in the Sichuan Basin, SW China. *Mar. Petrol. Geol.* **25**, 357-370.
Manger, G.E. (1963) Porosity and bulk density of sedimentary rocks, Bulletin, - ed, pp. 1-55.
Marty, B. (1984) On the noble gas, isotopic fractionation in naturally occurring gases. *Geol. J.* **18**, 157-162.
Matsuda, J., Matsumoto, T., Sumino, H., Nagao, K., Yamamoto, J., Miura, Y., Kaneoka, I., Takahata, N. and Sano, Y. (2002) The 3He/4He ratio of the new internal He Standard of Japan (HESJ). *Geol. J.* **36**, 191-195.
Ni, Y.Y., Dai, J.X., Tao, S.Z., Wu, X.Q., Liao, F.R., Wu, W. and Zhang, D.J. (2014) Helium signatures of gases from the Sichuan Basin, China. *Org. Geochem.* **74**, 33-43.
Onstott, T.C. and Tseng, H.Y. (1997) A tectogenetic origin for the deep subsurface microorganisms of Taylorsville Basin: thermal and fluid flow model constraints. *FEMS Microbiol. Rev.* **20**, 391-397.
Ozima, M. and Podosek, F.A. (2002) Noble gas geochemistry. *Cambridge University Press, Cambridge*.
Pinti, D.L. and Marty, B. (1995) Noble gases in crude oils from the Paris Basin, France: Implications for the origin of fluids and constraints on oil-water-gas interactions. *Geochim. Cosmochim. Ac.* **59**, 3389-3404.
Price, L.C., Blount, C.W., Gowan, D.M., Wenger, L., Bebout, D.G. and Bachman, A.L. (1981) Methane solubility in brines with application to the geopressured resource, United States, pp. 205-214.
Qin, S., Li, F., Zhou, Z. and Zhou, G. (2018) Geochemical characteristics of water-dissolved gases and implications on gas origin of Sinian to Cambrian reservoirs of Anyue gas field in Sichuan Basin, China. *Mar. Petrol. Geol.* **89**, 83-90.
Qin, S., Zou, C., Dai, J., Li, M., Hu, J., Zhang, Q. and Lu, Y. (2006) Water-soluble gas accumulation process of Hetianhe gas field in Tarim Basin, NW China. *Petrol. Explor. Dev.* **33**, 282-288.
Rudnick, R.L. and Fountain, D.M. (1995) Nature and composition of the continental crust: A lower crustal perspective. *Rev. Geophys.* **33**, 267-309.
Schlegel, M.E., Zhou, Z., McIntosh, J.C., Ballentine, C.J. and Person, M.A. (2011) Constraining the timing of microbial methane generation in an organic-rich shale using noble gases, Illinois Basin, USA. *Chem. Geol.* **287**, 27-40.
Schoell, M. (1980) The hydrogen and carbon isotopic composition of methane from natural gases of various origins. *Geochim. Cosmochim. Ac.* **44**, 649-661.
Schoell, M. (1988) Multiple origins of methane in the Earth. *Chem. Geol.* **71**, 1-10.
Smith, S.P. and Kennedy, B.M. (1983) The solubility of noble gases in water and in NaCl brine. *Geochim. Cosmochim. Ac.* **47**, 503-515.
Soest., M.C.v., T.Torgersen. and Kennedy., B.M. (2000) The Statfjord and Snorre Fields, Norwegian North Sea oil province. EOS, Trans. *Am. Geophys. Union* **81**, 442.
Stute, M., Clark, J.F., Schlosser, P., Broecker, W.S. and Bonani, G. (1995) A 30,000 yr Continental Paleotemperature Record Derived from Noble Gases Dissolved in Groundwater from the San Juan Basin, New Mexico. *Quat. Res.* **43**, 209-220.
Stute, M., Schlosser, P., Clark, J.F. and Broecker, W.S. (1992) Paleotemperatures in the Southwestern United States Derived from Noble Gases in Ground Water. *Science* **256**, 1000-1003.
Summa, L.L. (1995) Diagenesis and reservoir quality prediction. *Rev. Geophys.* **33**, 87-94.
Tan, X., Li, L., Liu, H., Luo, B., Zhou, Y., Wu, J. and Ding, X. (2011) General depositional features of the carbonate platform gas reservoir of the Lower Triassic Jialingjiang Formation

in the Sichuan Basin of southwest China: Moxi gas field of the central basin. *Carbonates and Evaporites* **26**, 339-350.
Tang, L., Guo, T., Jin, W., Yu, Y. and Li, R. (2008) Main Structural Styles and Deformation Mechanisms in the Northern Sichuan Basin, Southern China. *Acta Geologica Sinica - English Edition* **82**, 543-553.
Taylor, S.R. and McLennan, S.M. (1985) The Continental Crust: Its Composition and Evolution. *Geol. J.* **21**, 85-86.
Tian, H., Zhang, J., Xin, Y., Li, W. and Zhang, H. (2019) Reservoir characteristics and forming conditions for the Middle Triassic Leikoupo Formation in the western Sichuan Basin, China. *Journal of Natural Gas Geoscience* **4**, 101-110.
Tilley, B. and Muehlenbachs, K. (2006) Gas maturity and alteration systematics across the Western Canada Sedimentary Basin from four mud gas isotope depth profiles. *Org. Geochem.* **37**, 1857-1868.
Tilley, B. and Muehlenbachs, K. (2013) Isotope reversals and universal stages and trends of gas maturation in sealed, self-contained petroleum systems. *Chem. Geol.* **339**, 194-204.
Torgersen, T. (1980) Controls on pore-fluid concentration of 4He and 222Rn and the calculation of 4He/222Rn ages. *J. Geochem. Explor.* **13**, 57-75.
Torgersen, T. and Clarke, W.B. (1985) Helium accumulation in groundwater, I: An evaluation of sources and the continental flux of crustal 4He in the Great Artesian Basin, Australia. *Geochim. Cosmochim. Ac.* **49**, 1211-1218.
Torgersen, T. and Kennedy, B.M. (1999) Air-Xe enrichments in Elk Hills oil field gases: role of water in migration and storage. *Earth Planet. Sci. Lett.* **167**, 239-253.
Walvoord, M.A., Pegram, P., Phillips, F.M., Person, M., Kieft, T.L., Fredrickson, J.K., McKinley, J.P. and Swenson, J.B. (1999) Groundwater flow and geochemistry in the Southeastern San Juan Basin: Implications for microbial transport and activity. *Water Resour. Res.* **35**, 1409-1424.
Wang, H. (1985) Paleogeography of China. China Map Press, Beijing.
Wang, Y.P., Zhao, C.Y., Wang, H.J., Wang, Z.Y. and Wang, Z.C. (2013) Origins of natural gases from marine strata in Northeastern Sichuan Basin (China) from carbon molecular moieties and isotopic data. *J. Asian Earth Sci.* **65**, 13-20.
Warr, O., Sherwood Lollar, B., Fellowes, J., Sutcliffe, C.N., McDermott, J.M., Holland, G., Mabry, J.C. and Ballentine, C.J. (2018) Tracing ancient hydrogeological fracture network age and compartmentalisation using noble gases. *Geochim. Cosmochim. Ac.* **222**, 340-362.
Wei, G., Xie, Z., Song, J., Yang, W., Wang, Z., Li, J., Wang, D., Li, Z. and Xie, W. (2015) Features and origin of natural gas in the Sinian–Cambrian of central Sichuan paleo-uplift, Sichuan Basin, SW China. *Petrol. Explor. Dev.* **42**, 768-777.
Wei, G.Q., Chen, G.S., Du, S.M., Zhang, L. and Yang, W. (2008) Petroleum systems of the oldest gas field in China: Neoproterozoic gas pools in the Weiyuan gas field, Sichuan Basin. *Mar. Petrol. Geol.* **25**, 371-386.
Wei, G.Q., Wang, D.L., Wang, X.B., Li, J., Li, Z.S., Xie, Z.Y., Cui, H.Y. and Wang, Z.H. (2014) Characteristics of noble gases in the large Gaoshiti-Moxi gas field in Sichuan Basin, SW China. *Petrol. Explor. Dev.* **41**, 585-590.
Wen, T. (2017) Development of Noble Gas Techniques to Fingerprint Shale Gas and to Trace Sources of Hydrocarbons in Groundwater. *University of Michigan*.
Wen, T., Castro, M.C., Ellis, B.R., Hall, C.M. and Lohmann, K.C. (2015) Assessing compositional variability and migration of natural gas in the Antrim Shale in the Michigan Basin using noble gas geochemistry. *Chem. Geol.* **417**, 356-370.
Wen, T., Castro, M.C., Nicot, J.P., Hall, C.M., Pinti, D.L., Mickler, P., Darvari, R. and Larson, T. (2017) Characterizing the Noble Gas Isotopic Composition of the Barnett Shale

and Strawn Group and Constraining the Source of Stray Gas in the Trinity Aquifer, North-Central Texas. *Environ Sci Technol* **51**, 6533-6541.
Whiticar, M.J., Faber, E. and Schoell, M. (1986) Biogenic methane formation in marine and freshwater environments: CO2 reduction vs. acetate fermentation—Isotope evidence. *Geochim. Cosmochim. Ac.* **50**, 693-709.
Williams, L.B., Hervig, R.L. and Bjørlykke, K. (1997) New evidence for the origin of quartz cements in hydrocarbon reservoirs revealed by oxygen isotope microanalyses. *Geochim. Cosmochim. Ac.* **61**, 2529-2538.
Wise, D.L. and Houghton, G. (1968) Diffusion coefficients of neon, krypton, xenon, carbon monoxide and nitric oxide in water at 10–60°C. *Chem. Eng. Sci.* **23**, 1211-1216.
Xu, C., Shen, P., Yang, Y., Luo, B., Huang, J., Jiang, X., Xie, J. and Cen, Y. (2014) Accumulation conditions and enrichment patterns of natural gas in the Lower Cambrian Longwangmiao Fm reservoirs of the Leshan-Longnǚsi Palaeohigh, Sichuan Basin. *Nat. Gas Ind.* **1**, 51-57.
Yang, C., Ni, Z., Wang, T., Chen, Z., Hong, H., Wen, L., Luo, B. and Wang, W. (2018) A new genetic mechanism of natural gas accumulation. *Sci. Rep.* **8**, 8336.
Yang, Y., Wen, L., Luo, B., Wang, W. and Shan, S. (2016) Hydrocarbon accumulation of Sinian natural gas reservoirs, Leshan-Longnüsi paleohigh, Sichuan Basin, SW China. *Petrol. Explor. Dev.* **43**, 197-207.
Yuan, H.F., Liang, J.J., Gong, D.Y., Xu, G.S., Liu, S.G. and Wang, G.Z. (2012) Formation and evolution of Sinian oil and gas pools in typical structures, Sichuan Basin, China. *Petrol. Sci.* **9**, 129-140.
Zhai, G.M. (1989) Petroleum Geology of China. *Petroleum Industry Press, Beijing* **10**, 28-150.
Zhang, W., Li, Y., Zhao, F., Han, W., Li, Y., Wang, Y., Holland, G. and Zhou, Z. (2019) Using noble gases to trace groundwater evolution and assess helium accumulation in Weihe Basin, central China. *Geochim. Cosmochim. Ac.* **251**, 229-246.
Zhao, W., Hu, S., Xu, Z., Zeng, H., Liu, W., Fu, Q., Shi, S., Wang, L. and Jiang, L. (2018) Lithology mapping of a mixed siliciclastic−carbonate−evaporite system using 3D seismic and well data: Lower Triassic Jialingjiang Formation, Sichuan Basin, southwestern China. *Mar. Petrol. Geol.* **93**, 422-436.
Zhou, J., Xu, C., Yao, G., Yang, G., Zhang, J., Hao, Y., Wang, F., Pan, L., Gu, M. and Li, W. (2015) Genesis and evolution of Lower Cambrian Longwangmiao Formation reservoirs, Sichuan Basin, SW China. *Petrol. Explor. Dev.* **42**, 175-184.
Zhou, Z. and Ballentine, C.J. (2006) 4He dating of groundwater associated with hydrocarbon reservoirs. *Chem. Geol.* **226**, 309-327.
Zhou, Z., Ballentine, C.J., Kipfer, R., Schoell, M. and Thibodeaux, S. (2005) Noble gas tracing of groundwater/coalbed methane interaction in the San Juan Basin, USA. *Geochim. Cosmochim. Ac.* **69**, 5413-5428.
Zhou, Z., Ballentine, C.J., Schoell, M. and Stevens, S.H. (2012) Identifying and quantifying natural CO2 sequestration processes over geological timescales: The Jackson Dome CO2 Deposit, USA. *Geochim. Cosmochim. Ac.* **86**, 257-275.
Zhu, G., Zhang, S., Huang, H., Liang, Y., Meng, S. and Li, Y. (2011) Gas genetic type and origin of hydrogen sulfide in the Zhongba gas field of the western Sichuan Basin, China. *Appl. Geochem.* **26**, 1261-1273.
Zou, C.N. (2013) Unconventional Petroleum Geology, second ed. *Geology Press, Beijing*, 127-167.

Figure captions

Fig. 1. Geological features of the Sichuan Basin, China, and locations of sample collection sites in the Anyue gas field in the central Sichuan Basin (modified from Dai et al., 2012; Yuan et al., 2012 and Qin et al., 2018)

Fig. 2. Thermal history of well Anping 1, Anyue gas field, central Sichuan Basin (modified from Yuan et al., 2012). The dashed lines denote modelled hydrostatic temperature values. The vitrinite reflectance values (R_o) for Lower Cambrian Qiongzhusi ($Є_1q$) formation source rocks are also shown.

Fig. 3. Schematic diagram of the fully automated noble gas extraction line at Lancaster University (Li, 2019).

Fig. 4. $\delta^{13}C(CH_4)$ values measured in three different types of samples (free gases, water-dissolved gases and bitumen) in group 2 samples from the Longwangmiao formation of the Anyue gas field.

Fig. 5. $^3He/^4He$ ratios (R/R_a) versus $^4He/^{20}Ne$ ratios. R/R_a values measured in samples from group 1 and group 2 samples range from 0.0118 to 0.0132 and 0.0115 to 0.0256, respectively, suggesting strong contributions from the crust.

Fig. 6. $^{20}Ne/^{22}Ne$ vs. $^{21}Ne/^{22}Ne$ ratios for all samples in Anyue gas field. Neon ratios in all samples indicate a two-component mixing process between air and crust endmembers.

Fig. 7. $^{40}Ar/^{36}Ar$ ratios vs. $1/^{36}Ar$. $^{40}Ar/^{36}Ar$ ratios in all samples are significantly higher than the air value of 298.6 (Lee et al., 2006).

Fig. 8. Groundwater-derived noble gas abundances in Anyue gas field normalized to those of Air Saturated Water (ASW) at 10 °C with ^{36}Ar as the reference isotope.

Fig. 9. A) $^{4}He/^{40}Ar^{*}$ vs. $^{20}Ne^{\dagger}/^{36}Ar$ ratios, and B) $^{21}Ne^{*}/^{40}Ar^{*}$ vs. $^{4}He/^{40}Ar^{*}$ ratios in the Anyue gas field. The solid red and green lines are the solubility-controlled Rayleigh fractionation model lines in the gas phase for samples in group 1 and group 2, respectively. The dashed purple line is the diffusion-controlled fractionation model line for samples in both groups.

Fig. 10. A) $^{84}Kr/^{36}Ar$ vs. $^{20}Ne^{\dagger}/^{36}Ar$ ratios, and B) $^{132}Xe/^{36}Ar$ vs. $^{20}Ne^{\dagger}/^{36}Ar$ ratios measured in samples from the Anyue gas field. All the measured $^{84}Kr/^{36}Ar$ and $^{132}Xe/^{36}Ar$ ratios in gas samples are significantly above the predicted solubility-controlled Rayleigh fractionation line.

Fig. 11. ^{4}He ages of groundwater associated with the Longwangmiao formation of the Anyue gas field in Sichuan Basin. ^{4}He is assumed to be derived from a closed system (only in-situ production of ^{4}He is accumulated) and an open system (both in-situ production and external flux of ^{4}He are accumulated).

Fig. 12. Measured $CH_4/^{36}Ar$ ratios in the Anyue gas field as a function of depth. Two dotted lines show the expected $CH_4/^{36}Ar$ ratios in the CH_4 saturated pure water and 2M NaCl saline water, respectively.

Fig. 13. Cartoon illustrating the two-stage gas-groundwater interactions in the gas preservation and accumulation history of the Anyue gas field. Stage 1: (1.1) Hydrocarbon gases initially generated from oil-cracking have $\delta^{13}C$ values more negative than $\delta^{13}C$ in bitumen samples. (1.2) Water-dissolved gases with elevated $\delta^{13}C$ values higher than $\delta^{13}C$ in bitumen samples. (1.3) All noble gases together with some hydrocarbon gases have been lost due to lack of a stable trapping structure. (1.4) The gases accumulated in the current reservoir are mainly from gases exsolved from the original formation water with observed elevated $\delta^{13}C$ values higher than reservoir bitumen samples. Stage 2: (2.1) Noble gases derived from interaction with young meteoric groundwater are preserved in current reservoir. (2.2) Hydrocarbon gases dissolved in young meteoric groundwater have further elevated $\delta^{13}C$ values compared to free gases in the current reservoir.

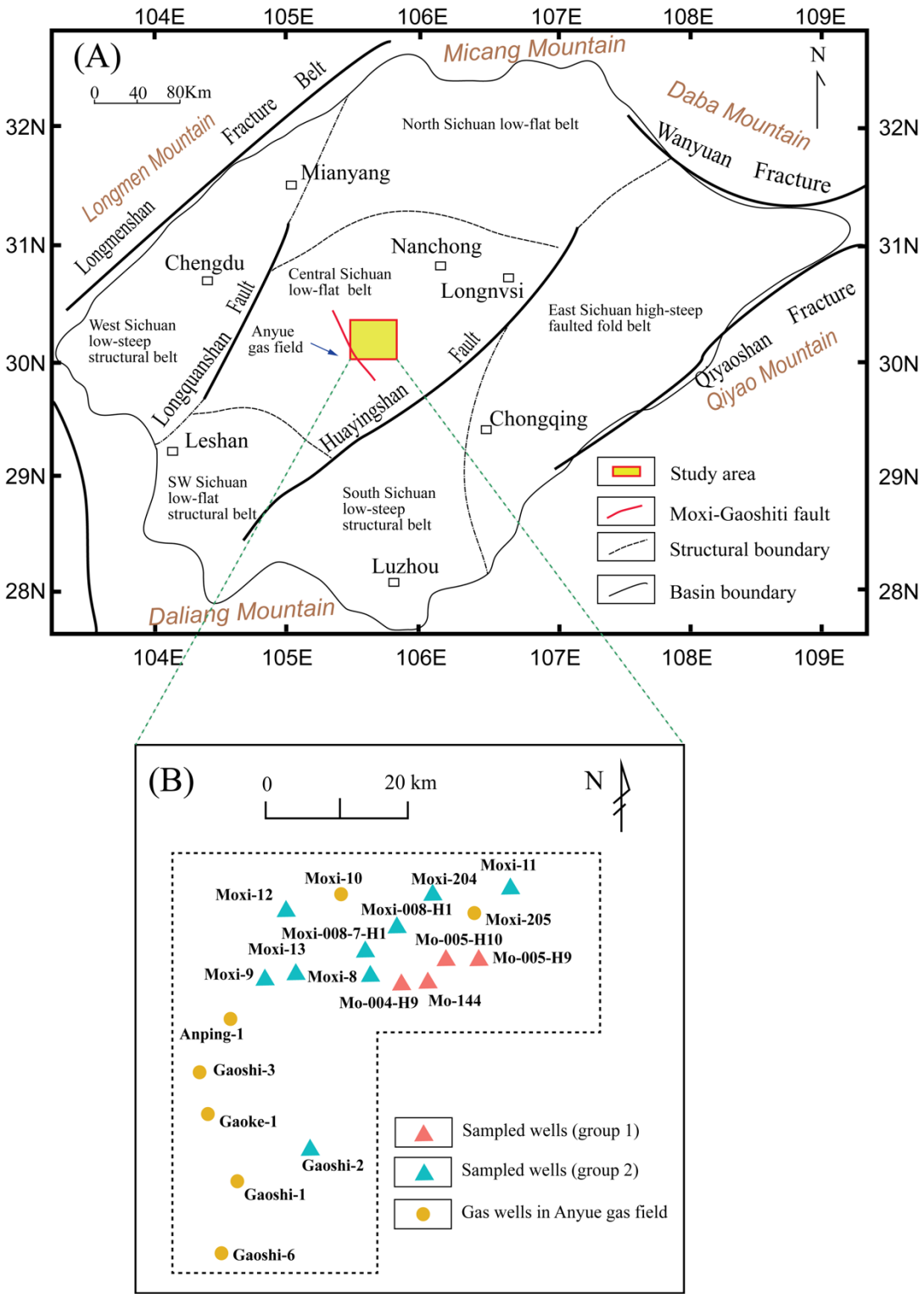
(A)
0 40 80Km
N
104E
105E
106E
107E
108E
109E
32N
31N
30N
29N
28N
Micang Mountain
Daba Mountain
Longmen Mountain
Longmenshan Fracture Belt
Wanyuan Fracture
North Sichuan low-flat belt
Mianyang
Chengdu
Nanchong
Longnvsi
Central Sichuan low-flat belt
West Sichuan low-steep structural belt
Anyue gas field
Longquanshan Fault
East Sichuan high-steep faulted fold belt
Huayingshan Fault
Qiyaoshan Fracture
Qiyao Mountain
Chongqing
Leshan
SW Sichuan low-flat structural belt
South Sichuan low-steep structural belt
Luzhou
Daliang Mountain
Study area
Moxi-Gaoshiti fault
Structural boundary
Basin boundary
(B)
0
20 km
N
Moxi-10
Moxi-204
Moxi-11
Moxi-12
Moxi-008-H1
Moxi-205
Moxi-008-7-H1
Mo-005-H10
Moxi-13
Mo-005-H9
Moxi-9
Moxi-8
Mo-004-H9
Mo-144
Anping-1
Gaoshi-3
Gaoke-1
Gaoshi-2
Gaoshi-1
Gaoshi-6
Sampled wells (group 1)
Sampled wells (group 2)
Gas wells in Anyue gas field

Figure 1

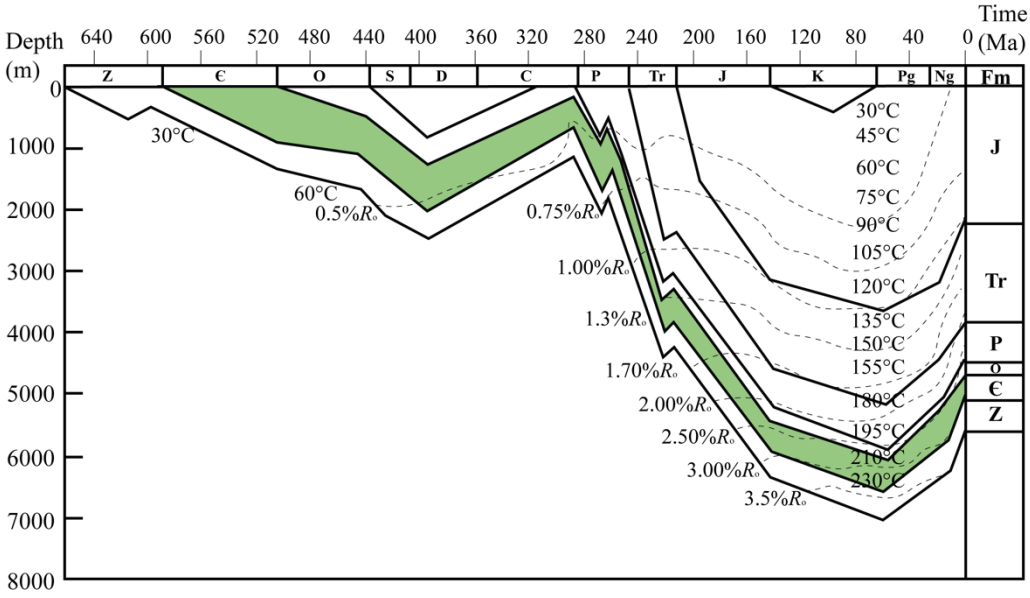
Depth
(m)
Time
(Ma)
640
600
560
520
480
440
400
360
320
280
240
200
160
120
80
40
0
Z
Є
O
S
D
C
P
Tr
J
K
Pg
Ng
Fm
0
1000
2000
3000
4000
5000
6000
7000
8000
30°C
60°C
0.5%Ro
0.75%Ro
1.00%Ro
1.3%Ro
1.70%Ro
2.00%Ro
2.50%Ro
3.00%Ro
3.5%Ro
30°C
45°C
60°C
75°C
90°C
105°C
120°C
135°C
150°C
155°C
180°C
195°C
210°C
230°C
J
Tr
P
O
Є
Z

Figure 2

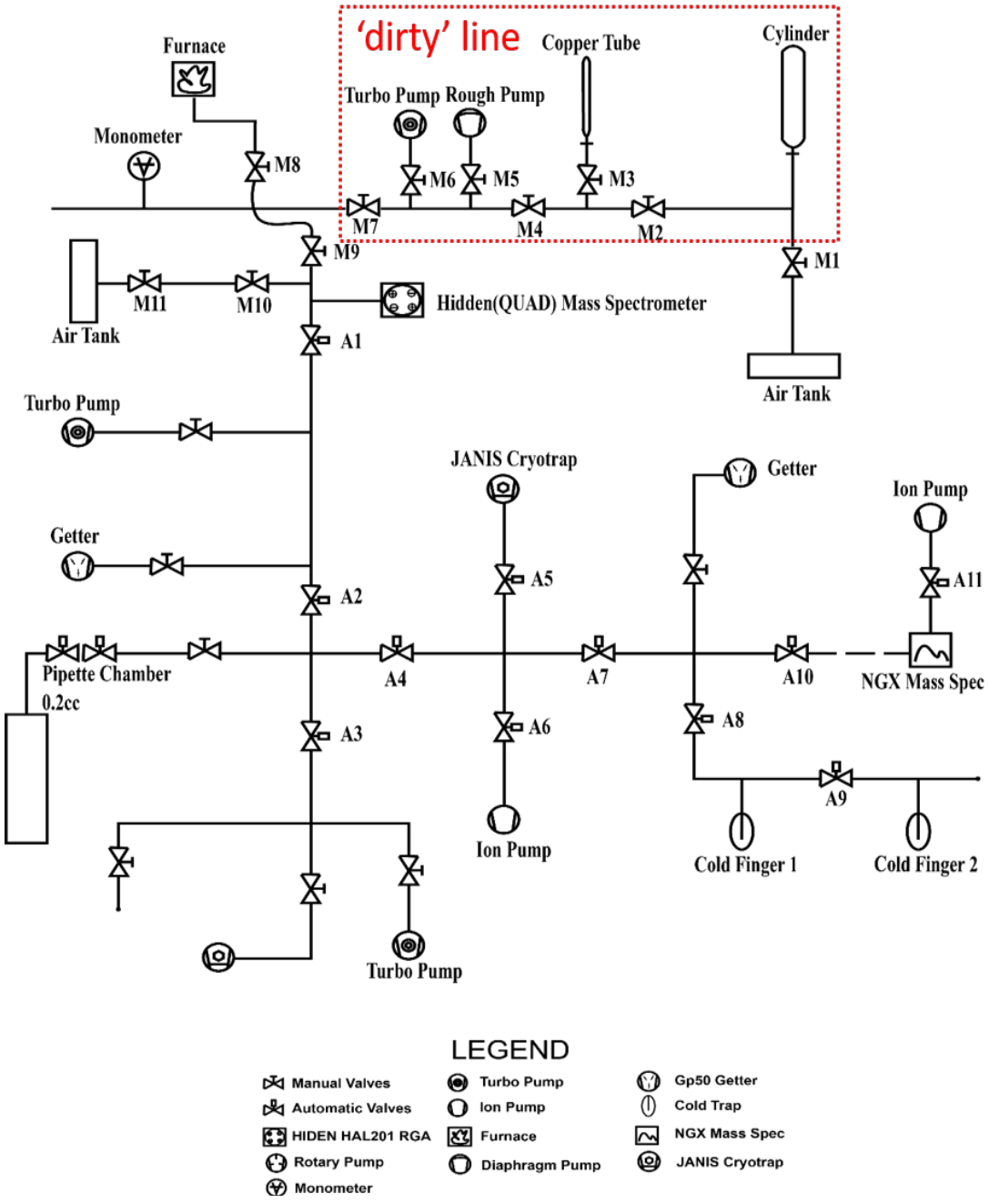
'dirty' line
Copper Tube
Cylinder
Furnace
Turbo Pump
Rough Pump
Monometer
M8
M6
M5
M3
M7
M4
M2
M9
M1
M11
M10
Hidden(QUAD) Mass Spectrometer
Air Tank
A1
Air Tank
Turbo Pump
JANIS Cryotrap
Getter
Ion Pump
Getter
A5
A11
A2
Pipette Chamber
0.2cc
A4
A7
A10
NGX Mass Spec
A3
A6
A8
A9
Ion Pump
Cold Finger 1
Cold Finger 2
Turbo Pump
LEGEND
Manual Valves
Automatic Valves
HIDEN HAL201 RGA
Rotary Pump
Monometer
Turbo Pump
Ion Pump
Furnace
Diaphragm Pump
Gp50 Getter
Cold Trap
NGX Mass Spec
JANIS Cryotrap

Figure 3

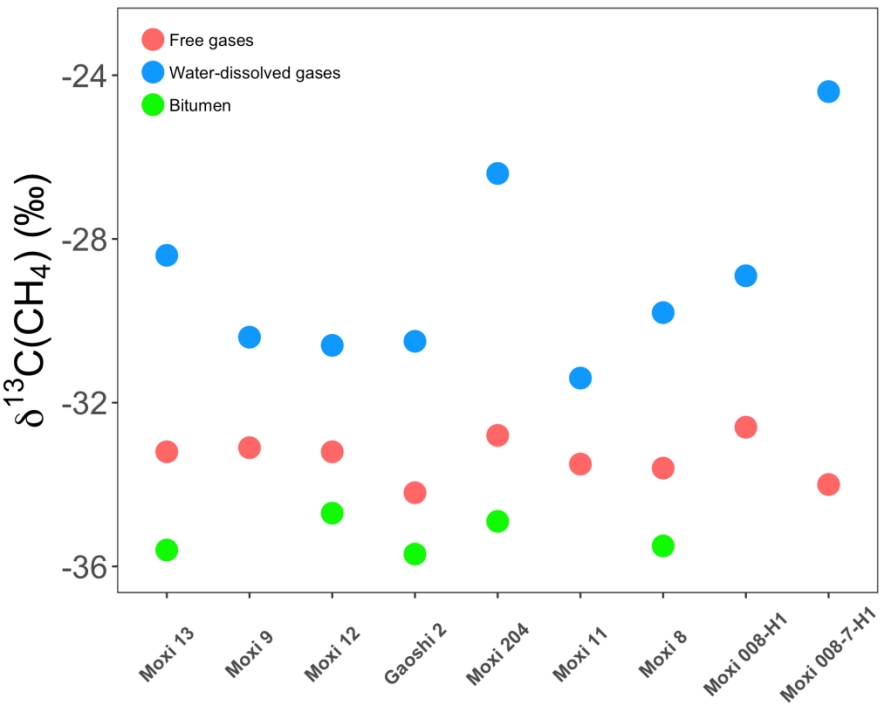
Free gases
Water-dissolved gases
Bitumen
-24
-28
-32
-36
δ13C(CH4) (‰)
Moxi 13
Moxi 9
Moxi 12
Gaoshi 2
Moxi 204
Moxi 11
Moxi 8
Moxi 008-H1
Moxi 008-7-H1

Figure 4

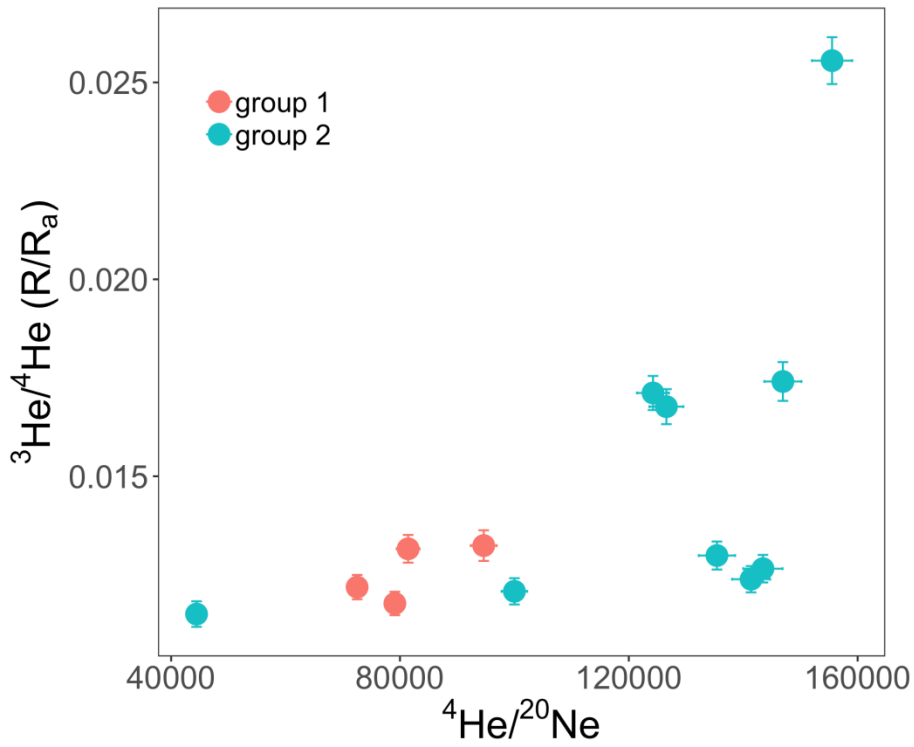
group 1
group 2
0.025
0.020
0.015
$^{3}He/^{4}He$ (R/R_a)
40000
80000
120000
160000
$^{4}He/^{20}Ne$

Figure 5

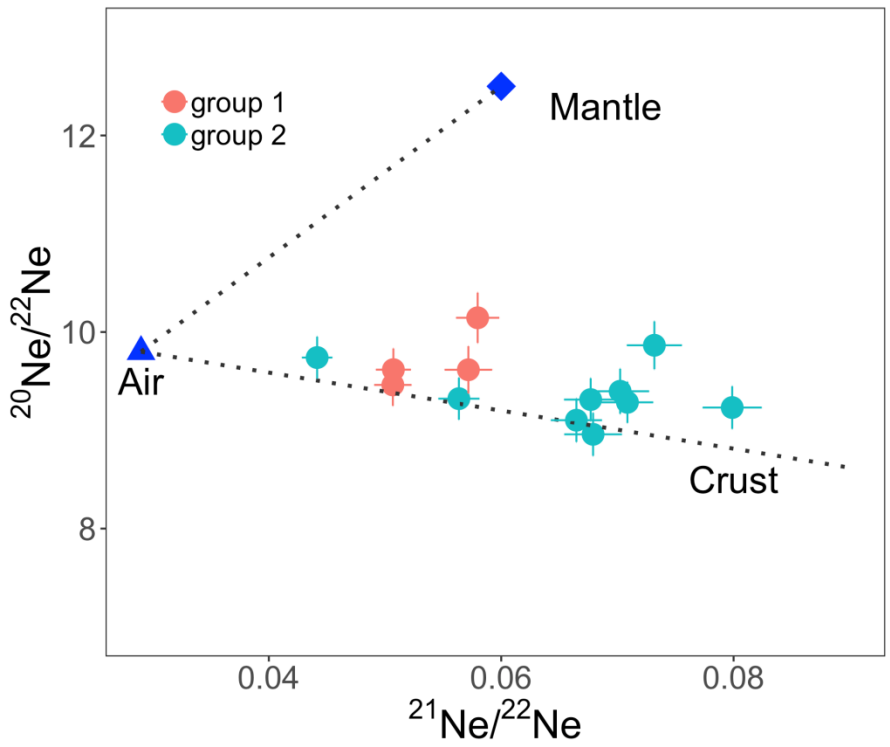
group 1
group 2
Mantle
Air
Crust
12
10
8
0.04
0.06
0.08
$^{20}Ne/^{22}Ne$
$^{21}Ne/^{22}Ne$

Figure 6

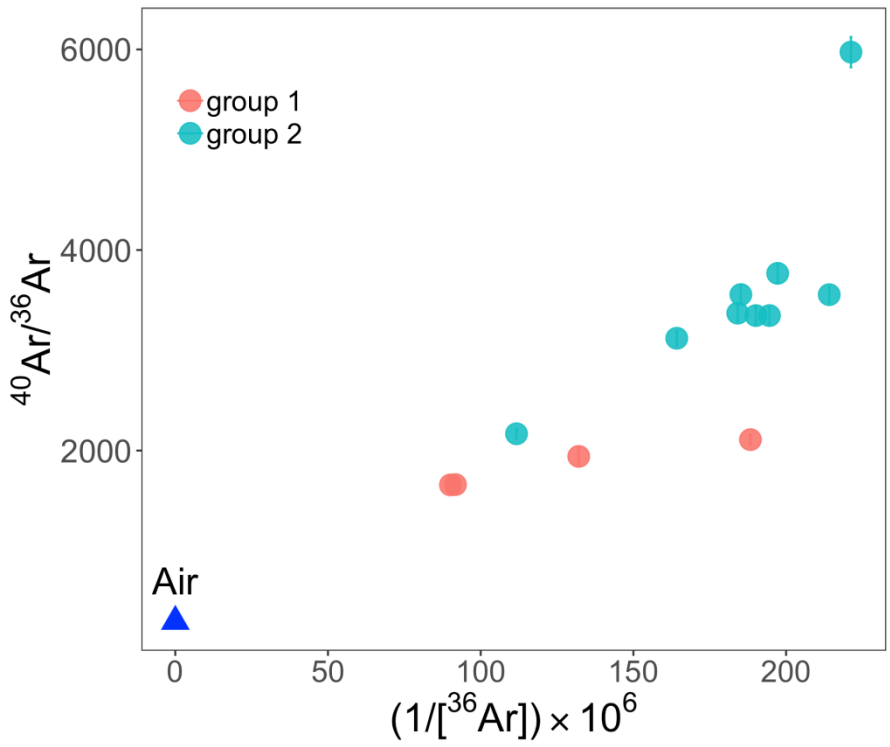
6000
4000
2000
group 1
group 2
Air
0
50
100
150
200
$^{40}Ar/^{36}Ar$
$(1/[^{36}Ar]) \times 10^6$

Figure 7

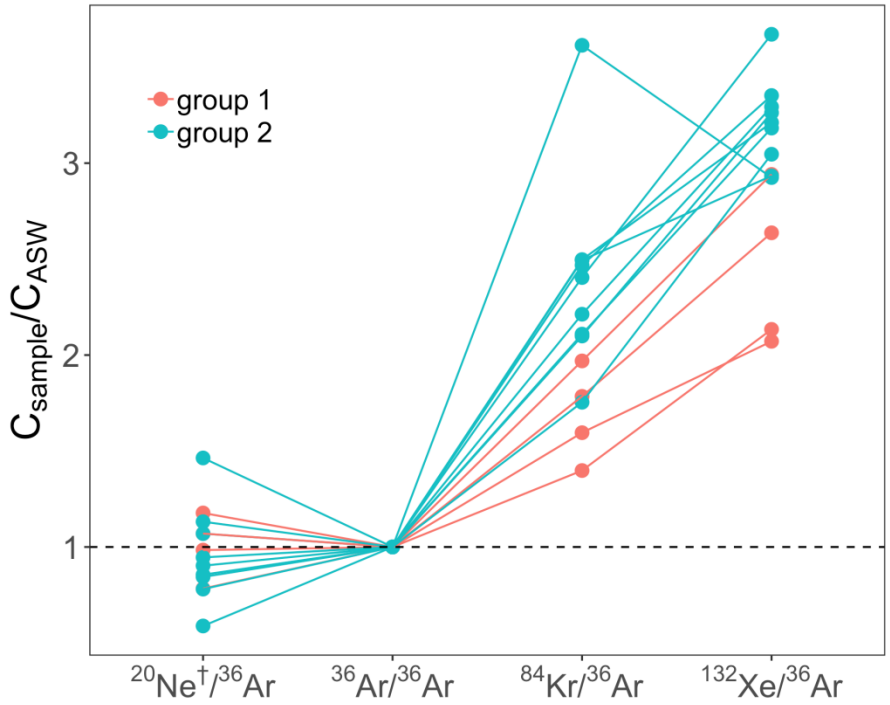
group 1
group 2
3
2
1
C_{sample}/C_{ASW}
$^{20}Ne^{\dagger}/^{36}Ar$
$^{36}Ar/^{36}Ar$
$^{84}Kr/^{36}Ar$
$^{132}Xe/^{36}Ar$

Figure 8

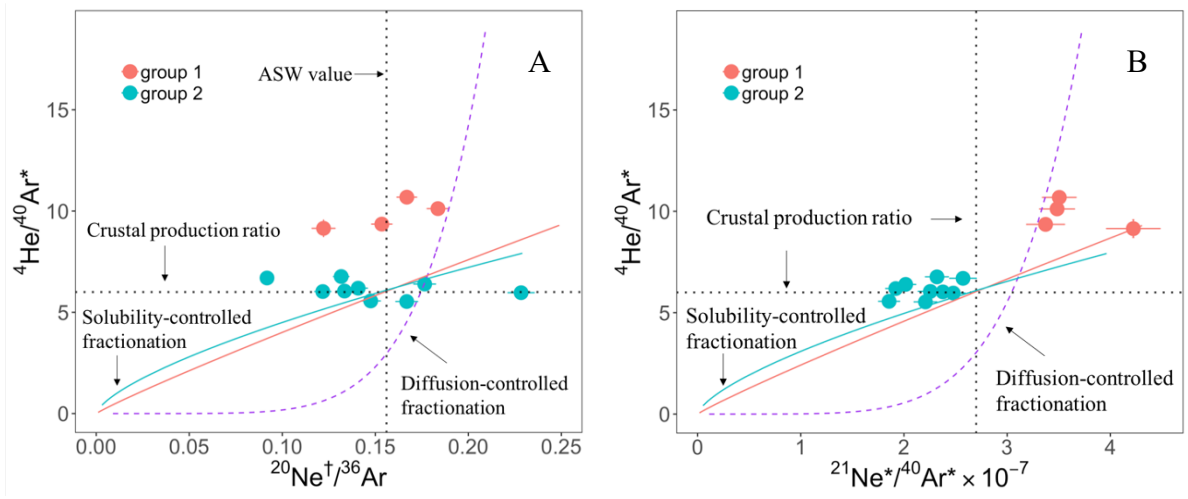
A
group 1
group 2
ASW value
Crustal production ratio
Solubility-controlled fractionation
Diffusion-controlled fractionation
$^4He/^{40}Ar^*$
$^{20}Ne^{\dagger}/^{36}Ar$
B
group 1
group 2
Crustal production ratio
Solubility-controlled fractionation
Diffusion-controlled fractionation
$^4He/^{40}Ar^*$
$^{21}Ne^*/^{40}Ar^* \times 10^{-7}$

Figure 9

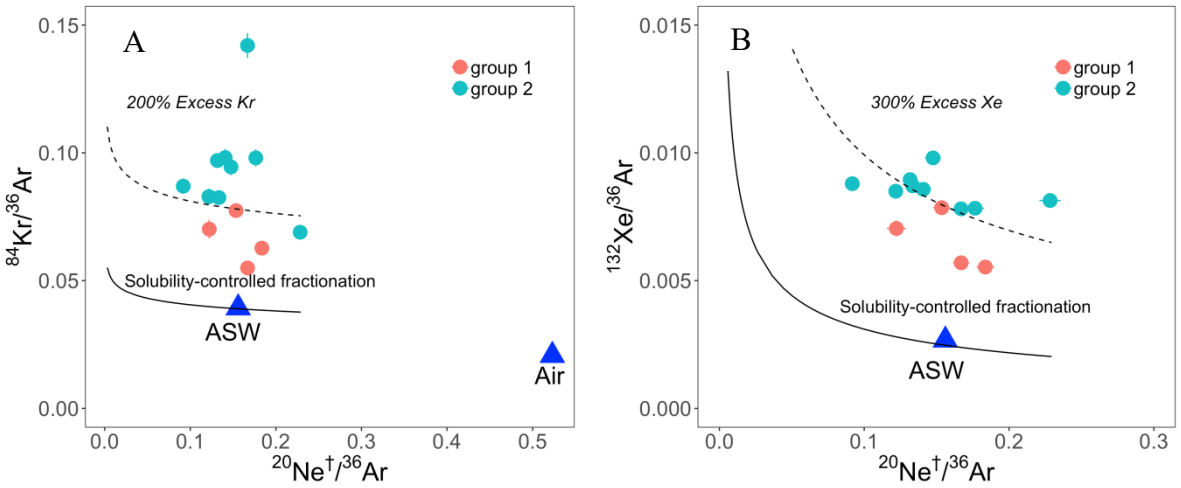
A
group 1
group 2
200% Excess Kr
Solubility-controlled fractionation
ASW
Air
0.15
0.10
0.05
0.00
0.0
0.1
0.2
0.3
0.4
0.5
84Kr/36Ar
20Ne†/36Ar
B
group 1
group 2
300% Excess Xe
Solubility-controlled fractionation
ASW
0.015
0.010
0.005
0.000
0.0
0.1
0.2
0.3
132Xe/36Ar
20Ne†/36Ar

Figure 10

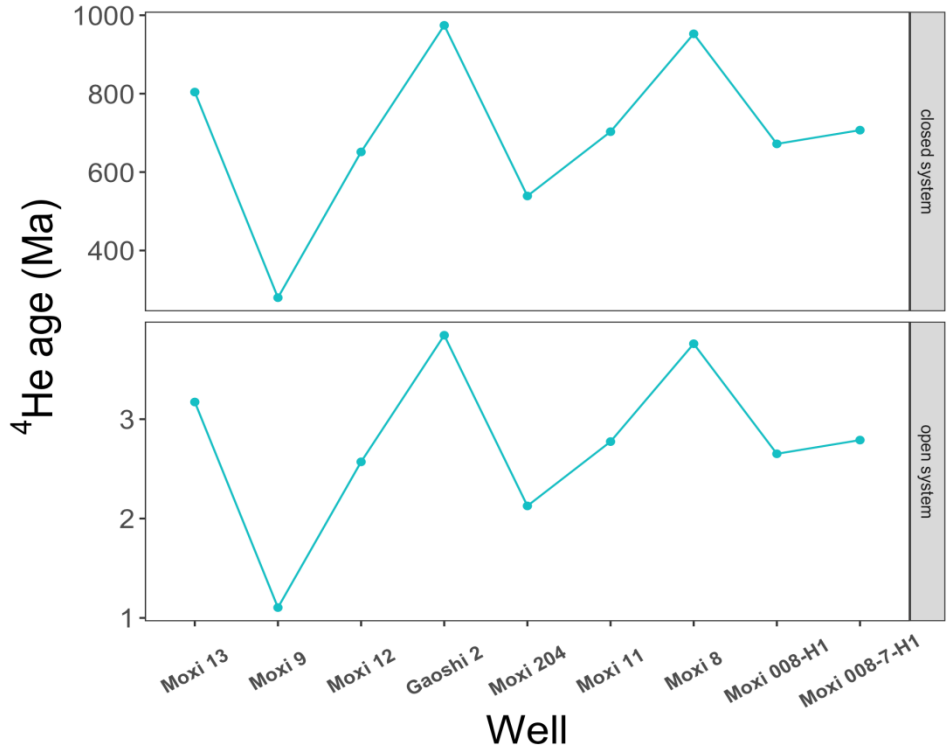
1000
800
600
400
3
2
1
^{4}He age (Ma)
closed system
open system
Moxi 13
Moxi 9
Moxi 12
Gaoshi 2
Moxi 204
Moxi 11
Moxi 8
Moxi 008-H1
Moxi 008-7-H1
Well

Figure 11

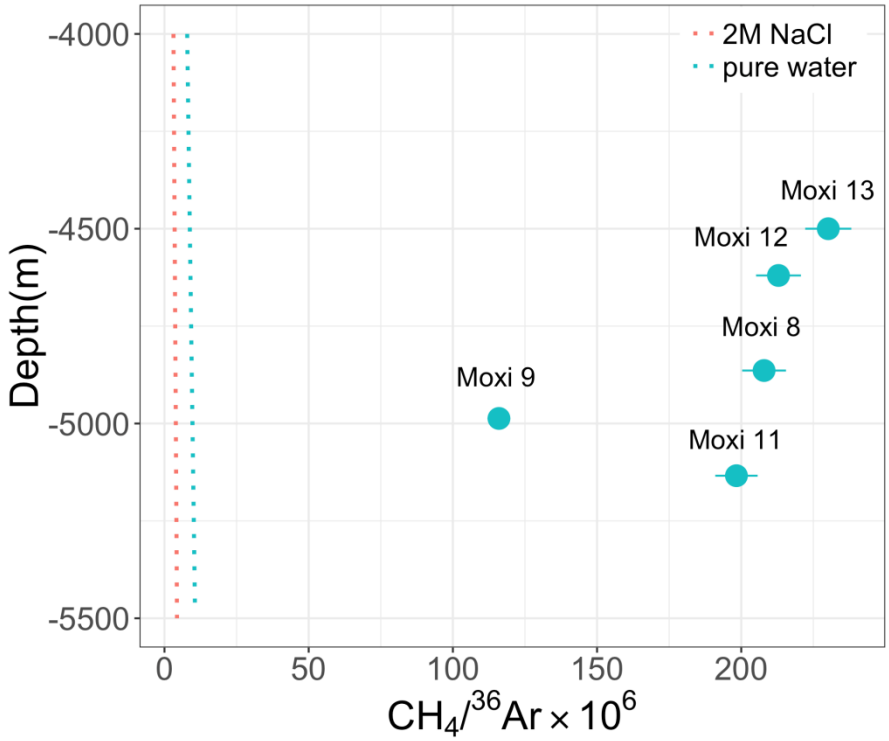
2M NaCl
pure water
Moxi 13
Moxi 12
Moxi 8
Moxi 9
Moxi 11
-4000
-4500
-5000
-5500
Depth(m)
0
50
100
150
200
CH4/36Ar × 10^6

Figure 12

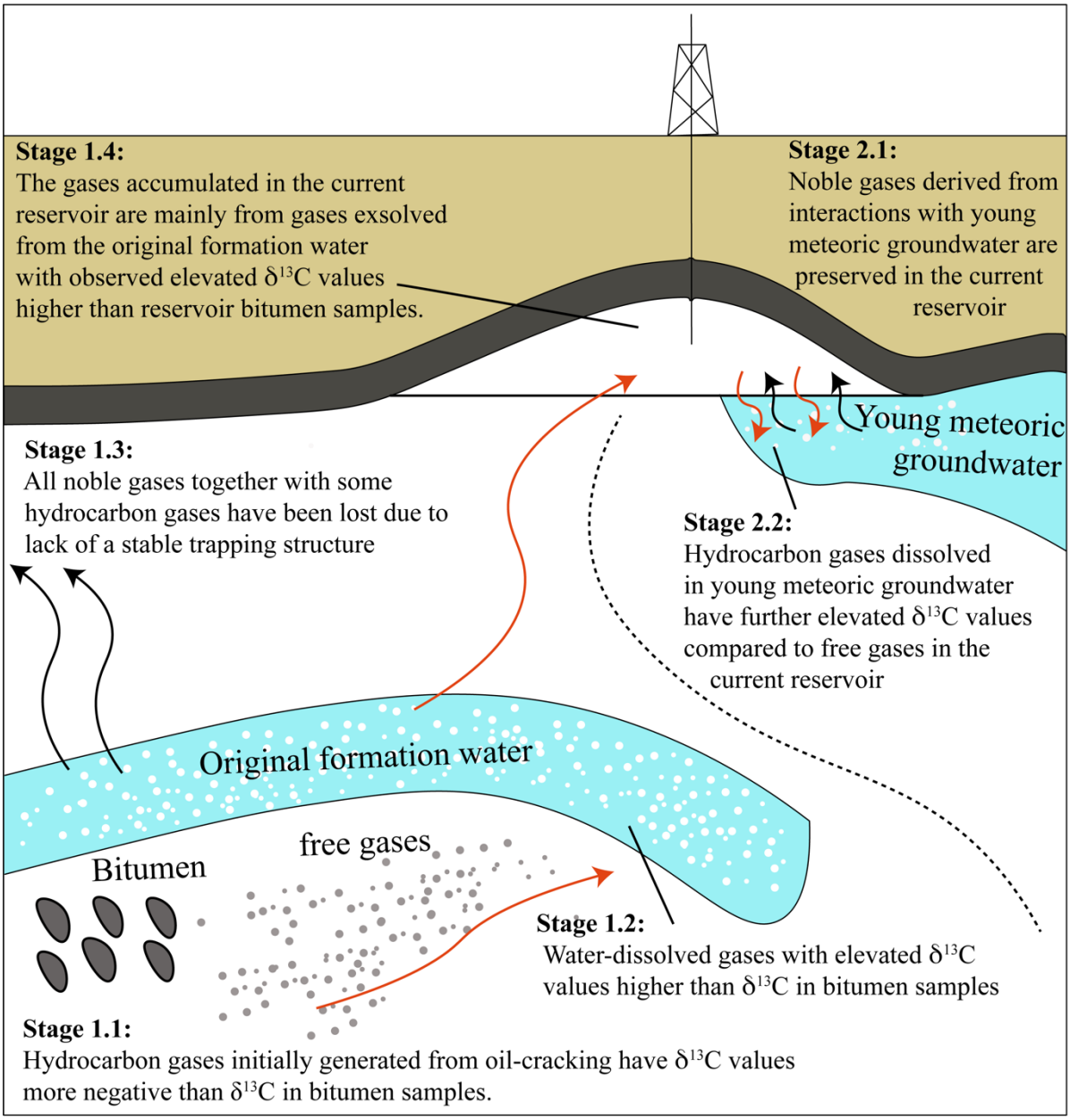
Stage 1.4:
The gases accumulated in the current reservoir are mainly from gases exsolved from the original formation water with observed elevated δ13C values higher than reservoir bitumen samples.
Stage 2.1:
Noble gases derived from interactions with young meteoric groundwater are preserved in the current reservoir
Young meteoric groundwater
Stage 1.3:
All noble gases together with some hydrocarbon gases have been lost due to lack of a stable trapping structure
Stage 2.2:
Hydrocarbon gases dissolved in young meteoric groundwater have further elevated δ13C values compared to free gases in the current reservoir
Original formation water
free gases
Bitumen
Stage 1.2:
Water-dissolved gases with elevated δ13C values higher than δ13C in bitumen samples
Stage 1.1:
Hydrocarbon gases initially generated from oil-cracking have δ13C values more negative than δ13C in bitumen samples.

Figure 13

Table 1

Major gas species and stable carbon isotopes in the Anyue gas field in central Sichuan Basin, China

Well	Depth (m)	Gas composition (%)					C1/C1-C5	Stable isotopes		
		CH_4 (±2%)	C_2H_6 (±2%)	CO_2 (±2%)	O_2 (±2%)	N_2 (±2%)		$\delta^{13}C(CH_4)$ (±0.2‰) VPDB[b]	$\delta^{13}C(C_2)$ (±0.2‰) VPDB	$\delta^{13}C(C_3)$ (±0.2‰) VPDB
group 1										
Mo 144	NA	98.90	0.18	0.00	0.16	0.75	0.9982	-34.9	-32.1	NA
Mo 004-H9	NA	99.12	0.16	0.00	0.13	0.59	0.9984	-35.0	-32.8	NA
Mo 005-H9	NA	98.81	0.19	0.00	0.18	0.81	0.9981	-34.8	-33.6	NA
Mo 005-H10	NA	99.24	0.21	0.00	0.10	0.44	0.9979	-34.6	-34.6	NA
group 2										
Moxi 13	4500[a]	99.09	0.11	0.15	0.00	0.65	0.9989	-33.2	-31.5	NA
Moxi 9	4987[a]	99.14	0.09	0.05	0.00	0.73	0.9991	-33.1	-31.6	-25.9
Moxi 12	4620[a]	98.96	0.11	0.35	0.00	0.58	0.9989	-33.2	-31.9	NA
Gaoshi 2	NA[*]	98.92	0.04	0.38	0.00	0.66	0.9996	-34.2	-30.5	-25.4
Moxi 204	NA	99.87	0.13	0.07	0.00	0.66	0.9987	-32.8	-31.5	-26.0
Moxi 11	5134[a]	98.73	0.12	0.20	0.00	0.95	0.9988	-33.5	-31.5	NA
Moxi 8	4864[a]	99.05	0.14	0.21	0.00	0.60	0.9986	-33.6	-32.5	NA
Moxi 008-H1	NA	99.32	0.13	0.22	0.00	0.33	0.9987	-32.6	-32.2	-29.3
Moxi 008-7-H1	NA	99.20	0.13	0.25	0.00	0.41	0.9987	-34.0	-32.1	NA

[a] Data cited from Liu et al. (2015)

[b] The stable carbon isotopic values were reported in the δ notation in per mil (‰) relative to the Peedee belemnite standard (VPDB). Reproducibility and accuracy were estimated to be ±0.2‰ with respect to VPDB standard.

[*] NA-Not Available

Table 2

Sample strata and noble gas concentrations in the Anyue gas field in central Sichuan Basin, China

Well	Strata	^{4}He ($\times10^{-5}$) cm^3STP/cm^3	^{20}Ne ($\times10^{-10}$) cm^3STP/cm^3	$^{20}Ne^{\dagger}$ ($\times10^{-10}$)[b] cm^3STP/cm^3	^{40}Ar ($\times10^{-5}$) cm^3STP/cm^3	^{36}Ar ($\times10^{-9}$) cm^3STP/cm^3	^{84}Kr ($\times10^{-10}$) cm^3STP/cm^3	^{132}Xe ($\times10^{-11}$) cm^3STP/cm^3
group 1								
Mo144	T_2l_1[a]	15.30±0.22	21.10±0.36	20.38±0.57	1.84±0.03	11.10±0.18	6.96±0.19	6.14±0.11
Mo 004-H9	T_2l_1	15.90±0.23	20.10±0.34	18.19±0.51	1.81±0.03	10.90±0.18	5.99±0.15	6.21±0.12
Mo 005-H9	T_1J_2[a]	11.40±0.16	14.00±0.28	9.25±0.30	1.47±0.02	7.57±0.31	5.31±0.17	5.33±0.10
Mo 005-H10	T_1J_2	9.01±0.13	9.52±0.18	8.15±0.26	1.12±0.02	5.31±0.10	4.11±0.13	4.17±0.08
group 2								
Moxi 13	ϵ_1l[a]	10.30±0.15	7.01±0.12	6.15±0.17	1.66±0.02	4.67±0.08	4.53±0.11	4.18±0.07
Moxi 9	ϵ_1l	10.00±0.14	22.50±0.36	20.44±0.56	1.94±0.03	8.95±0.15	6.17±0.16	7.28±0.12
Moxi 12	ϵ_1l	9.79±0.14	7.23±0.14	7.48±0.23	1.91±0.03	5.07±0.10	4.79±0.14	4.97±0.09
Gaoshi 2	ϵ_1l	14.20±0.20	9.13±0.16	7.54±0.22	2.70±0.04	4.52±0.10	6.42±0.18	3.53±0.07
Moxi 204	ϵ_1l	11.00±0.16	11.00±0.19	10.75±0.31	1.90±0.03	6.09±0.11	5.97±0.18	4.77±0.09
Moxi 11	ϵ_1l	10.90±0.15	7.71±0.14	7.60±0.23	1.92±0.03	5.40±0.11	5.30±0.15	4.63±0.08
Moxi 8	ϵ_1l	10.50±0.15	7.32±0.14	4.72±0.15	1.72±0.02	5.14±0.10	4.47±0.13	4.52±0.09
Moxi 008-H1	ϵ_1l	10.10±0.14	8.13±0.14	7.25±0.21	1.83±0.03	5.43±0.11	4.48±0.13	4.73±0.09
Moxi 008-7-H1	ϵ_1l	9.67±0.14	7.64±0.14	6.40±0.20	1.76±0.02	5.26±0.11	4.36±0.14	4.47±0.09
Air[c]		0.524	165000		930	31420	6500	2340

[a] T_2l_1, T_1J_2 and ϵ_1l denote the first member of Middle Triassic Leikoupo formation, the second member of Lower Triassic Jialingjiang formation and Lower Cambrian Longwangmiao formation.

[b] $^{20}Ne^{\dagger}$ denotes groundwater-derived ^{20}Ne.

[c] Ozima and Podosek (2002)

Table 3

Noble gas isotopic compositions and groundwater-derived and radiogenic noble gas elemental compositions in the Anyue gas field in central Sichuan Basin, China

well	$^{3}He/^{4}He$ (R/Ra)	$^{20}Ne/^{22}Ne$	$^{21}Ne/^{22}Ne$	$^{40}Ar/^{36}Ar$	$^{38}Ar/^{36}Ar$	$^{86}Kr/^{84}Kr$	$^{136}Xe/^{132}Xe$	$^{4}He/^{21}Ne^{*}$ ($\times10^{7}$)	$^{20}Ne^{\dagger}/^{36}Ar$	$^{4}He/^{40}Ar^{*}$	$^{21}Ne^{*}/^{40}Ar^{*}$[a] ($\times10^{-7}$)
group 1											
Mo144	0.0122±0.0003	9.46±0.21	0.0507±0.0016	1658±35	0.188±0.006	0.320±0.017	0.3257±0.0100	2.90±0.13	0.184±0.006	10.12±0.30	3.48±0.17
Mo 004-H9	0.0118±0.0003	9.62±0.22	0.0507±0.0015	1661±36	0.189±0.006	0.332±0.015	0.3349±0.0104	3.05±0.13	0.167±0.005	10.69±0.32	3.51±0.17
Mo 005-H9	0.0132±0.0004	10.14±0.26	0.0580±0.0019	1942±83	0.176±0.008	0.347±0.019	0.3265±0.0102	2.17±0.10	0.122±0.006	9.15±0.43	4.22±0.26
Mo 005-H10	0.0132±0.0004	9.62±0.24	0.0572±0.0021	2109±49	0.198±0.008	0.353±0.022	0.3213±0.0104	2.77±0.14	0.153±0.006	9.36±0.29	3.37±0.19
group 2											
Moxi 13	0.0174±0.0005	9.28±0.21	0.0709±0.0022	3555±80	0.190±0.006	0.313±0.015	0.3301±0.0091	2.92±0.13	0.132±0.004	6.77±0.20	2.32±0.12
Moxi 9	0.0115±0.0003	9.74±0.21	0.0442±0.0013	2168±47	0.187±0.006	0.327±0.017	0.3297±0.0091	2.41±0.10	0.228±0.007	5.97±0.18	2.48±0.12
Moxi 12	0.0130±0.0004	8.96±0.22	0.0679±0.0025	3767±90	0.185±0.007	0.311±0.017	0.3300±0.0100	3.00±0.15	0.148±0.005	5.56±0.17	1.86±0.11
Gaoshi 2	0.0256±0.0006	9.23±0.22	0.0799±0.0025	5973±151	0.193±0.009	0.304±0.016	0.3399±0.0109	2.51±0.11	0.167±0.006	5.53±0.18	2.21±0.11
Moxi 204	0.0121±0.0003	9.32±0.21	0.0564±0.0018	3120±73	0.186±0.007	0.295±0.017	0.3333±0.0107	3.17±0.14	0.177±0.006	6.40±0.20	2.02±0.10
Moxi 11	0.0124±0.0003	9.10±0.22	0.0665±0.0022	3556±86	0.181±0.007	0.296±0.017	0.3218±0.0103	3.22±0.15	0.141±0.005	6.19±0.19	1.92±0.10
Moxi 8	0.0127±0.0004	9.87±0.24	0.0732±0.0024	3346±80	0.182±0.008	0.315±0.018	0.3341±0.0104	2.60±0.12	0.092±0.003	6.70±0.21	2.57±0.13
Moxi 008-H1	0.0171±0.0004	9.31±0.22	0.0677±0.0023	3370±81	0.190±0.007	0.308±0.018	0.3277±0.0099	2.68±0.13	0.133±0.005	6.05±0.19	2.26±0.12
Moxi 008-7-H1	0.0168±0.0004	9.40±0.23	0.0702±0.0025	3346±84	0.198±0.008	0.298±0.017	0.3266±0.0099	2.53±0.13	0.122±0.005	6.03±0.19	2.38±0.13
Air[b]	1	9.80	0.029	298.6[c]	0.1880	0.305	0.3293	0.00001	0.524	0.00056	52.4

[a] $^{21}Ne^{*}$ and $^{40}Ar^{*}$ denote non-atmospheric ^{21}Ne and ^{40}Ar, respectively.

[b] Ozima and Podosek (2002)

[c] Lee et al. (2006)

Table 4

Predicted initial ^{4}He concentrations in the groundwater in the Longwangmiao formation of the Anyue gas field

well	group	$(^{20}Ne/^{36}Ar)_{water}$	f	$(^{4}He/^{36}Ar)_{water}$	$(^{4}He/^{36}Ar)_{initial}$	The initial ^{4}He concentrations in the water (cm^3 STP/cm^3 H_2O)
Moxi 13	group 2	0.090	0.307	1.67×10^{4}	2.44×10^{4}	1.84×10^{-2}
Moxi 9[a]	group 2	0.156	0.994	8.47×10^{3}	8.49×10^{3}	6.41×10^{-3}
Moxi 12	group 2	0.100	0.391	1.46×10^{4}	1.98×10^{4}	1.49×10^{-2}
Gaoshi2	group 2	0.114	0.509	2.38×10^{4}	2.96×10^{4}	2.23×10^{-2}
Moxi 204	group 2	0.120	0.573	1.37×10^{4}	1.64×10^{4}	1.24×10^{-2}
Moxi 11	group 2	0.096	0.354	1.53×10^{4}	2.13×10^{4}	1.61×10^{-2}
Moxi 8	group 2	0.063	0.142	1.55×10^{4}	2.89×10^{4}	2.18×10^{-2}
Moxi 008-H1	group 2	0.091	0.315	1.41×10^{4}	2.04×10^{4}	1.54×10^{-2}
Moxi 008-7-H1	group 2	0.083	0.259	1.39×10^{4}	2.14×10^{4}	1.62×10^{-2}

Table 5
^{4}He accumulation rates in groundwater and the parameters used for calculations

	Strata	U (ppm)	Th (ppm)	Density (g/cm^3)	Porosity (%)	Thickness (m)	Accumulation rate (in situ)	Accumulation rate (external)
Anyue[a]	C_1l	3.8	9.8	2.7	8	50	2.29×10^{-11}	5.79×10^{-9}
Crust[b]	Upper	2.8	10.7	2.6		12300		
	Lower	0.28	1.07	3.3		36900		

[a] U and Th contents estimated from Le (2015). Porosity and density values derived from Manger (1963).Thickness value cited from Du et al. (2014)
[b] U and Th contents derived from Taylor and McLennan (1985). Density and Thickness values derived from Taylor and McLennan (1985) and Zhou and Ballentine (2006)